Division of Pharmaceutical Chemistry and Technology
Faculty of Pharmacy
University of Helsinki
Finland

Toward accurate high-throughput physicochemical profiling using image-based single-particle analysis

by

Sami Svanbäck

ACADEMIC DISSERTATION

To be presented, with the permission of the Faculty of Pharmacy of the University of Helsinki, for public examination in Auditorium 1, Infocenter Korona (Viikinkaari 11), on July 15th 2016, at 12.00 noon.

Helsinki 2016

Supervisors Professor Jouko Yliruusi
Division of Pharmaceutical Chemistry and Technology
Faculty of Pharmacy
University of Helsinki
Finland

Dr. Henrik Ehlers
Division of Pharmaceutical Chemistry and Technology
Faculty of Pharmacy
University of Helsinki
Finland

Reviewers Professor Jyrki Heinämäki
Institute of Pharmacy
Faculty of Medicine
University of Tartu
Estonia

Professor Niklas Sandler
Department of Biosciences
Faculty of Science and Engineering
Åbo Akademi University
Finland

Opponent Professor Thomas Rades
Department of Pharmacy
University of Copenhagen
Denmark

ISBN 978-951-51-2297-1 (Paperback)
ISBN 978-951-51-2298-8 (PDF)
ISSN 1799-7372

Helsinki University Printing House
Helsinki 2016

Abstract

Svanbäck, S., 2016. **Toward accurate high-throughput physicochemical profiling using image-based single-particle analysis.**

Dissertationes Scholae Doctoralis Ad Sanitatem Investigandam Universitatis Helsinkiensis, 48/2016, pp. 53
ISBN 978-951-51-2297-1 (Paperback), ISBN 978-951-51-2298-8 (PDF, http://ethesis.helsinki.fi), ISSN 1799-7372

Key physicochemical properties determining the developability of a drug include solubility, dissolution rate, lipophilicity and pK_a. Not only do these properties affect synthesis and solid form optimization, choice of administration route, processability and formulation strategies; they also greatly influence, directly or indirectly, the absorption, distribution, metabolism, excretion, toxicity and efficacy of drugs. However, miniaturized methods that would enable small-scale determination of these fundamental properties in an accurate and rapid way, are lacking. Image-based microscopy could provide an opportune method for non-specific, rapid and miniaturized applications.

First, the applicability of image-based microscopy and single-particle analysis in drug dissolution rate measurement was evaluated. This was done by comparing image analysis data with traditional UV spectrophotometric data of individual dissolving drug pellets. It was found that dissolution rates obtained by image analysis and UV spectrophotometry were practically identical.

Next, a single-particle trap flow-through device was developed, wherein it is possible to continuously monitor individual drug particles under constant flow conditions. Based on the promising results of image-based dissolution rate analysis, the possibility of acquiring the intrinsic dissolution rate from individual freely rotating particles, trapped inside the flow through device, was evaluated. It was found that image analysis can be used for rapid real-time determination of intrinsic dissolution rates from continuously changing effective surface areas of dissolving individual micro-particles.

The method was then further extended to determine the equilibrium solubility of drugs. Based on the diffusion layer dissolution rate model, solubility is the rate limiting factor of dissolution and can therefore be determined. While solubility is generally determined from bulk solutions after long incubation times, it was shown that the equilibrium solubility can be rapidly determined from individual pure-substance particles by means of the diffusion layer theory and image analysis.

Finally, the single-particle method was further miniaturized and a second device developed, in order to allow imaging of individual powder crystals. It was shown that dissolution rate and solubility can be acquired from individual nanogram crystals. The single-particle method was further extended to acquire pK_a, *logP* and *logD* of the studied substances, using aqueous buffers, simulated physiological solutions and organic solvents. Using this method and device, it is possible to acquire a complete pH-solubility profile for an unknown material of unknown composition, with individual measurements of less than 30 seconds.

In summary, these results strongly suggest that image-based analysis of materials could be applied in high-throughput experimentation (HTE) applications. The possibility of acquiring solubility, dissolution rate, lipophilicity and pK_a using a single analytical method, could significantly simplify and speed up accurate data acquisition. This in turn, could lead to faster and more informed decision-making and, ultimately, better and more affordable drugs.

Acknowledgements

This is the last part of my thesis that I write and it turned out to be the most difficult one. Actually, to make any justice to these past few years, they should be written down in a thesis of their own. In all the busyness one rarely has the time to sit down and reflect, and then suddenly when starting to write one becomes aware of all the things that have passed. So many new people, so many new friends, so many places and countries and so many experiences. And there on the side, somehow this thesis has also materialized. Of all these memories; which and whom should I mention? As these are the acknowledgements for a thesis, I will focus on acknowledging those who have been most instrumental to the production and completion of this work.

The work for this thesis was carried out at the Division of Pharmaceutical Chemistry and Technology, Faculty of Pharmacy, University of Helsinki during the years 2013-2016 and made possible by a grant from the University of Helsinki Doctoral Programme in Drug Research.

I would like to start by extending my most sincere gratitude to my supervisor, mentor and friend Prof. Jouko Yliruusi. It's funny how our meetings tend to stray off topic and end up in long discussions and debates about everything and anything. Now looking back, these discussions have been the most rewarding and impactful of the past few years; thoughts and wisdom I will carry with me for the rest of my life. After being a bit lost about my education I was truly lucky to end up under your supervision and guidance. In the same way that you always remember to mention your great Professor K. V. Laurikainen, I will be reminding anyone and everyone far in the future about my great Professor Jouko Yliruusi.

I would also like to extend my deepest gratitude to my other supervisor Dr. Henrik Ehlers. You were the always available hands-on help and support during this project. I greatly admire your organizatory skills and sense for detail. Any time I needed something in the lab, be it a person, equipment, tool or part, you were the one to ask. And if not immediately found, it wouldn't be long before people were mobilized and it was effectively located; help was always close by. Your guidance in the writing process will also surely be reflected in all my future academic writing.

I am deeply indebted to my co-author Docent Osmo Antikainen. Your always relaxed and laughing attitude makes working a lot more fun. I thank you for your help in teaching me the secrets of coding and data analysis. Surely, this thesis would never have been finished without your help, instead I would still be manually analyzing those thousands and thousands of single-particle images (and probably going even more insane).

I am also deeply indebted to the technical support of Heikki Räikkönen. Without your assistance, none of the devices would have been built. If I ran into any kind of problem during my tinkering in the lab, you would always find a solution. You help and support and the countless discussions we have had have been truly teaching and rewarding.

I am thankful to Professor Jyrki Heinämäki, University of Tartu, and Professor Niklas Sandler, Åbo Akademi University, for reviewing this thesis and presenting constructive comments for its improvement.

I would like to extend my deep gratitude to Professor Edward Haeggström. The tough discussions that we have had have made me grow as a person and I am grateful for all the support and help you have given me during these years. I know you know it's not easy to herd cats. I would also like to acknowledge the collegiality of the rest of the Matteus team: Dr. Kai Falck, Ilkka Lassila and Antti Meriläinen. In particular I would like to thank Jenni Pessi. It is truly a pleasure working with you. Any time I forgot a measurement, you were there to cover and vice versa. Outside the lab your superhuman knowledge about organization and restaurants/bars (anywhere in the world!) always manages to amaze me.

I would also like to thank all my colleagues from the Division of Pharmaceutical Chemistry and Technology. Especially I would like to express my deepest gratitude to Associate Professor Clare Strachan. No matter how busy you were, you always managed to make time for helping and supporting me. Your language check was of great help for the overall coherence of this thesis. Also, you make excellent travel company and I will never forget that ordeal and aftermath of our trip home from the AAPS in 2015. I would also like to thank Dunja Novakovic, Emmi Palomäki, Jaana Hautala, Dr. Luis Bimbo, Markus Selin and Tiina Lipiäinen for your company and many rewarding discussions in the lab and at lunchtime. Jaana, I never laughed so much with anyone on a trip, before or after, as I did with you on our trip to the AAPS in 2014. In addition, I would like to thank all the exchange students that have come and gone. Especially I am thankful to Kristian Semjonov, Robert Lang, Stijn van Landeghem, Sylvie Langeraert, Carolina Alves and Jernej Štukelj.

A special mention go to Jukka Saarinen and Tuomas Saarinen. I was supposed to start writing these acknowledgements during our road trip with Jukka, but we were so busy traveling we barely had time to eat. Jukka, our shared passion for classic rock music has been enormously rewarding. I have found new music, learnt rock history and been to so many gigs and concerts that it is hard to remember all. The highlight was of course Ritchie Blackmore's Rainbow (twice), the main purpose of our road trip. Also, our twice monthly electric guitar sessions have been highlights and a way to detach from all the work and buzz. Long live Rock 'n' Roll! Tuomas, our discussions over a coffee or on the golf course have been very helpful and supportive. It is great to once in a while vent the air with someone in a similar position.

I was privileged to supervise two master's thesis workers during my PhD. Emma Hokkala and Anu Piipponen, you were my guinea pigs so thank you for bearing with me. I was lucky to get such good students and I learnt a lot about myself while supervising you; what to do and certainly what to do better with future victims.

I would like to express my deepest gratitude to Docent Hélder A. Santos for your support and kindness. Your dedication to science is truly admirable and something I wish I can one day emulate. Also, your ability to find great people has allowed me to make many lifetime friends. I want to thank everyone in Santos lab, for your friendship and collegiality. So much fun and so many laughs in and outside the lab. Especially I would like to thank (in alphabetical order) Alexandra Correia, Dr. Bárbara Herranz-Blanco, Dr. Dongfei Liu, Eloy Ginestar, Flavia Fontana, João Pedro Martins, Dr. Mohammad-Ali Shahbazi, Mónica Ferreira, Patrick Almeida, Patricia Figueiredo, Ricardo Rosa, Sérgio Almeida, Tomás Ramos and Dr. Vimalkumar Balasubramanian. I thank all of you for your assistance and friendship. Bárbara and Dongfei, your assistance regarding the thesis and preparations for the defense helped me to avoid most of the main pitfalls. Eloy, so many great discussions about technology, ideas and life. Your exceptional kindness and relaxed attitude toward life is something I admire a lot. Tomás and Ricardo, your exchange time in Helsinki made the start of my PhD life very smooth and enjoyable. Those months were some of the most fun and memorable of my entire PhD. In you and now also in João, I know I have a few more friends for life. Mónica, you are one of the people in my life that I admire most. Your kindness, integrity and trustworthiness makes you a friend I will never let go. Patrick, what a character and another friend for life. I don't know anyone, except you, who would be crazy enough to get up at five in the morning to go golfing with me. Also, your exceptional cooking skills have brought me much enjoyment during these years. Sérgio and Sara, the happiest couple I have met. I know that you, Sérgio, will never stop making people laugh, a true talent. Also, you introduced me to an equal comedian talent, Islam Faress. Like Behrouz Derakhshan you, Islam, will leave us soon, but I'm sure we will stay in contact. Without this great pack of people my life in and outside the lab would have been so

much less enjoyable. A special thanks also to all the Portuguese for patiently teaching me your strange but beautiful language.

I would also like to thank my friends Arttu, Eero, Jussi, Nicolas, Olli, Panu, Pyry and Tuomas. Especially I am indebted to my oldest friend Nicolas for our endless discussions and to Olli for always reminding me in my busyness to meet and relax for a while. Now before this gets completely out of hand I would like to end with the last and biggest acknowledgement. If you were not mentioned but reading this, know that you have had an impact on my life and that you matter to me.

In closing I would like to extend the biggest gratefulness to my family. To my cousin Eva for always asking and being interested in my undertakings. To my brother Mika for your continuous support and for bringing Erika into our family. And, lastly, to my mother Vellamo and my father Guy for your unconditional support and love. You pushed me where I didn't dare to go myself and brought my feet back on the ground when I was flying in the clouds. Without your support and guidance I would not be in the privileged position to write these words, I can never thank you enough.

Helsinki, June 2016.
Sami Svanbäck

Tietä käyden tien on vanki.
Vapaa on vain umpihanki.

-Aaro Hellaakoski

A prisoner of the road you tread you'll be.
Only the untrodden snowdrift is free.

-Aaro Hellaakoski (free translation)

Tärkeintä elämässä on puutarhanhoito,
eikä sekään ole kovin tärkeätä.

-Kiinalainen sananlasku

The most important thing in life is gardening,
and even that is not very important.

-Chinese proverb

But I, being poor, have only my dreams;
I have spread my dreams under your feet;
Tread softly because you tread on my dreams.

-W.B. Yeats

To my family

Table of contents

List of original publications

This thesis is based on the following publications, which are referred to in the text by their respective roman numerals (**I-IV**).

I **Svanbäck, S.**, Ehlers, H., Yliruusi, J., Optical microscopy as a comparative analytical technique for single-particle dissolution studies. International Journal of Pharmaceutics, 469: 10–16, 2014.

II **Svanbäck, S.**, Ehlers, H., Antikainen, O., Yliruusi, J., On-chip optofluidic single-particle method for rapid microscale equilibrium solubility screening of biologically active substances. Analytical Chemistry, 87: 5041–45, 2015.

III **Svanbäck, S.**, Ehlers, H., Antikainen, O., Yliruusi, J., High-speed intrinsic dissolution rate in one minute using the single-particle intrinsic dissolution rate method. Analytical Chemistry, 87: 11058–64, 2015.

IV **Svanbäck, S.,** Ehlers, H., Antikainen, O., Yliruusi, J., Toward femtogram resolution high-content physicochemical profiling of materials. Submitted, 2016.

Abbreviations and symbols

A	Surface area
a_-	Ionic radius of negative ion
a_+	Ionic radius of positive ion
ADME	Absorption, distribution, metabolism and excretion
ADMET	Absorption, distribution, metabolism, excretion and toxicity
API	Active pharmaceutical ingredient
ASA	Acetylsalicylic acid
BCS	Biopharmaceutics classification system
c	Circularity
CCD	Charge coupled device
CE	Capillary electrophoresis
CMOS	Complementary metal-oxide-semiconductor
C_t	Concentration at time t
D_c	Diffusion coefficient
dC/dt	Change in concentration with time
DIDR	Disc-intrinsic dissolution rate
dM/dt	Mass released per time
DMSO	Dimethyl sulfoxide
e	Elementary charge
ε	Dielectric constant
ε_o	Vacuum permittivity
f_1	Difference factor
f_2	Similarity factor
FaSSGF	Fasted state simulated gastric fluid
FaSSIF	Fasted state simulated intestinal fluid
FeSSIF	Fed state simulated intestinal fluid
fps	Frames per second
γ	Interfacial energy/surface tension
GI	Gastrointestinal
GSE	General solubility equation
h	Diffusion layer thickness
HBA	Hydrogen bond acceptor
HBD	Hydrogen bond donor
HCA	High-content analysis
HPLC	High-performance liquid chromatography
HTE	High-throughput experimentation
HTS	High-throughput screening
IC_{50}	Half maximal inhibitory concentration
IDR	Intrinsic dissolution rate
k, K	Dissolution rate constants
k_B	Boltzmann constant
K_i	Inhibition constant
k_s	System constant
LELP	Ligand-efficiency-dependent lipophilicity
LLE	Lipophilic ligand efficiency

logD	Logarithm of the distribution coefficient
logP	Logarithm of the partition coefficient
μ	Chemical potential
μ^i	Energy per molecule
MITT	Mean intestinal transit
MS	Mass spectrometry
MS/MS	Tandem mass spectrometry
MW	Molecular weight
NME	New molecular entity
NROT	Number of rotatable bonds
P	Permeation
p	Perimeter
PBS	Phosphate-buffered saline
PCM	Paracetamol
PIDR	Powder-intrinsic dissolution rate
PK	Pharmacokinetics
pK_a	Ionization constant
PSA	Polar surface area
QSAR	Quantitative structure activity relationship
QSPR	Quantitative structure property relationship
ρ	Density
R^2	Coefficient of determination
R&D	Research and development
RGB	Red, green and blue
RMSE	Root mean square error
ROI	Region of interest
%RSD	Relative standard deviation
S	Equilibrium solubility
S_o	Intrinsic solubility
sd	Standard deviation
SEM	Scanning electron microscopy
SGA	Spectral gradient analysis
SIDR	Single-particle-intrinsic dissolution rate
S_N	Native solubility
S_{oct}	Solubility in octanol
S_W	Solubility in water
T	Absolute temperature in Kelvin
t	Time
TP	Theophylline
V	Volume
w_o	Initial weight of particle
w_t	Weight of particle at time t
X	Concentration
X_S	Saturation concentration in mole fractions
Å	Ångström = 0.1 nm

1 Introduction

The process of bringing an new molecular entity (NME) to the market requires approximately 13.5 years with estimated research and development (R&D) costs in the range of US $0.8 billion to US $2.7 billion (Paul *et al.* 2010; Munos 2009; Kola & Landis 2004; DiMasi *et al.* 2003). These costs have been growing exponentially for the past 60 years reaching US $50 billion in collective annual R&D spending during the last years (Paul *et al.* 2010; Munos 2009). Simultaneously, R&D productivity has not been growing at the same rate, with the number of approved new drugs remaining essentially constant during this period (Munos 2009). However, following a decade of decreasing NME output, R&D productivity has been showing signs of recovery during the last years, with a new high for the past two decades of 45 approved new drugs on the US market in 2015 (Mullard 2016; Smietana *et al.* 2015).

Nonetheless, a concurrent decrease in the actual and forecasted sales as well as a strong public and political pressure on decreasing drug spending, will undoubtedly reduce the R&D returns of this recent positive upswing in productivity (Smietana *et al.* 2015; Munos 2009; Kola & Landis 2004). In an environment of intense competition the pharmaceutical industry is thus continuously forced to find new ways to increase R&D productivity and returns (Cook *et al.* 2014; Paul *et al.* 2010; Munos 2009; Kola & Landis 2004; DiMasi 2002). The fact that the pharmaceutical industry has not been able to increase the NME output since the 1950s, while R&D spending has soared, indicates that the rate of innovation has been barely enough to sustain the R&D process (Munos 2009).

In order to reduce R&D costs, a bolder implementation of novel technologies and practices that result in faster development, through more informed decision-making regarding development projects, is required (Smietana *et al.* 2015; Munos 2009; DiMasi 2002). An increase in R&D productivity in turn will bring higher returns to the companies and ultimately cheaper drugs to patients, as returns translate into new R&D investments, thus affecting the output and price of new medicines (Kola & Landis 2004; DiMasi 2002). Currently only around 11% of NMEs entering the development process make it through to regulatory approval and only 30% of these recover their initial R&D investment (Kola & Landis 2004).

The pharmaceutical industry is on the other hand highly and increasingly regulated, making the implementation of novel practices more challenging (Paul *et al.* 2010; Munos 2009). This is especially true for the expensive later clinical (Phase II and Phase III) stages of the development process (Paul *et al.* 2010). However, the preclinical and drug discovery phases are favorable for implementation of new technologies, as the information produced during these phases is mostly intended for in-house decision making, avoiding the requirement for regulatory compliance. The disproportional distribution of resources toward late-stage development, instead of the earlier discovery research phase has been identified as one of the possible root causes of the poor R&D productivity of the last decade (Paul *et al.* 2010). The benefit of a more efficient preclinical drug discovery phase is twofold: first, it accounts for 32% of NME development costs; second, and more importantly, it will reduce downstream attrition and costs accrued by later stage development failures (Smietana *et al.* 2015; Paul *et al.* 2010; Kola & Landis 2004; Gardner *et al.* 2004; DiMasi 2002).

However, quality cannot be sacrificed for quantity regarding the data produced by novel technologies introduced for early decision-making (Cook *et al.* 2014; Paul *et al.* 2010). For example, the vastly increased number of leads generated by high-throughput screening (HTS) and combinatorial chemistry did not translate into an increase in NME output (Cook *et al.* 2014; Alsenz & Kansy 2007). Instead, it led to increasing R&D costs and increasingly poor physicochemical properties, such as low solubility and high lipophilicity and molecular weight (MW) of candidate development compounds (Alsenz & Kansy 2007; Gardner *et al.* 2004).

A shift toward higher quality and more holistic data acquisition has therefore been introduced into the R&D decision-making process (Cook *et al.* 2014; Alsenz & Kansy 2007; Leeson & Springthorpe 2007; Gardner *et al.* 2004). Key physicochemical properties determining the developability of a drug include pK_a, solubility, dissolution rate and lipophilicity. These properties not only affect synthesis and solid form optimization, choice of administration route, processability and formulation strategies; they also greatly influence the pharmacokinetics [PK = absorption, distribution, metabolism and excretion (ADME)] of a compound (Waring 2010; Tong *et al.* 2009; Alsenz & Kansy 2007; Gardner *et al.* 2004; Merkle & Jen 2002; Kerns 2001). Furthermore, these parameters are determinants of pharmacological efficacy, and are directly and indirectly connected to safety issues as well as NME attrition (Morgan *et al.* 2012; Gleeson 2008; Alsenz & Kansy 2007; Leeson & Springthorpe 2007).

Current state of the art methods for physicochemical characterization of drugs have not been able to provide reliable means for high throughput experimentation (HTE). Especially for solubility measurement, there appears to be a discrepancy between throughput, substance consumption and accuracy. Instead, computational methods are used in early discovery, due to the lack of experimental methods capable of accommodating the requirements for throughput and low materials consumption (Tetko *et al.* 2009; Gardner *et al.* 2004). These *in silico* methods are, however, often inaccurate and challenging to implement due to the vast dimensionality of the possible chemical space of drug molecules (Balogh *et al.* 2012; Tetko *et al.* 2009; Mannhold *et al.* 2009; Jorgensen & Duffy 2002). The biggest issue with *in silico* models is, however, that they rely on experimental input parameters for accurate prediction.

This dissertation focuses on investigating and implementing image-based microscopy as a potential analytical method for physicochemical characterization of drugs. The non-specificity and potential for rapid data acquisition with automated analysis, makes image-based analysis a promising method for accurate high-speed applications. In addition, two new miniaturized flow-through devices are introduced in this work. By means of these devices it is demonstrated that fundamental physicochemical properties, such as solubility, dissolution rate, lipophilicity and pK_a can be determined from individual particles, in a fast, robust and cost-efficient way.

2 Review of the literature

2.1 Physicochemical equilibria and kinetics

In the simplest terms, the distribution of molecules and particles between two regions, phases or states in a system is described by the Boltzmann distribution (Israelachvili 1992). At equilibrium, the total free energy per molecule or particle, known as the chemical potential (μ), in the system is uniform,

$$\mu_1 = \mu_2 \tag{1}$$

and the Boltzmann distribution is expressed as,

$$\mu_1^i + k_B T ln X_1 = \mu_2^i + k_B T ln X_2 \tag{2}$$

where μ_1^i and μ_2^i are the energies and X_1 and X_2 are the concentrations of the molecules or particles in the two regions, phases or states in the system, k_B is the Boltzmann constant and T is the absolute temperature (Israelachvili 1992).

In this chapter the three generally expressed thermodynamic equilibria, in relation to drug molecules, will be presented. These are the ionization constant, solubility and partition/distribution coefficient. In addition to these, the kinetic rate of dissolution, which is a physicochemical property widely applicabile to drugs, will be presented. The reader should bear in mind that the equations presented in this chapter are often approximate, semiempirical and limited to ideal systems and, therefore, only model simple cases such as monoprotic acids and bases, monovalent salts and nonelectrolytes in simple solvents. The intent here is, however, not to give a comprehensive review, but to convey the general basis of and the relationships between the most central physicochemical properties, revisited in later chapters of this thesis.

2.1.1 Charge state

Most drug molecules are weak acids or bases and their charge state, *i.e.* degree of dissociation in solvents, will therefore strongly depend on the *pH* of the solvent (Avdeef 2001). The ratio between dissociated and undissociated species will further have implications on other kinetic and thermodynamic parameters as will be reviewed in subsequent chapters. The thermodynamic constant describing the acid-base equilibrium is called the ionization constant (pK_a). The pK_a is the *pH* at which the concentrations of the dissociated and undissociated species are equal and is expressed by the well-known Henderson-Hasselbalch relations,

$$pK_a = pH + log\left(\frac{[HA]}{[A^-]}\right) \tag{3}$$

for an acid and,

$$pK_a = pH + log\left(\frac{[BH^+]}{[B]}\right) \quad (4)$$

for a base, where the symbols within brackets denote the concentration of the dissociated and undissociated species of the acid *HA* and base *B*, respectively.

2.1.2 Solubility

Solubility is the thermodynamic equilibrium determined by the opposite kinetic rates of dissolution and precipitation at constant volume, pressure and temperature (Kerns & Di 2008; Sugano *et al.* 2007; Bhattachar *et al.* 2006). In the simplest way, solubility can be expressed by the Boltzmann distribution (Eq. 2) as the state where the chemical potential of molecules in the solid and dissolved molecules in the liquid is uniform,

$$X_S = exp\left[\frac{-(\mu_2^i - \mu_1^i)}{k_B T}\right] \quad (5)$$

where X_S denotes the saturation concentration in mole fractions (Israelachvili 1992). Starting from the Boltzmann distribution a General Solubility Equation (GSE) for the solubility of a nonelectrolyte in water (S_W) has been derived,

$$logS_W = 0.5 - logP - 0.01(MP - 25) \quad (6)$$

where MP is the melting point of the dissolving solid in degrees Celcius (Jain & Yalkowsky 2001; Ran *et al.* 2001; Yalkowsky & Valvani 1980). The partition coefficient (*logP*) is used here to describe the difference in polarity between the solute and water, *i.e.* the anticipated strength of adhesive interactions, and MP is used as a measure of the energy required to dissociate molecules and break the cohesive forces in the crystal lattice (Jain and Yalkowsky 2001). The magnitude of the difference between the adhesive and cohesive forces will generally be predictive of the solubility. The solubility of a dissociated salt is more complex and can be expressed by the Boltzmann distribution (Eq. 2) as,

$$X_S = exp\left[\frac{-e^2}{4\pi\varepsilon_0\varepsilon(a_+ + a_-)k_B T}\right] \quad (7)$$

where e is the elementary charge, ε_0 is the vacuum permittivity, ε is the dielectric constant of the solvent and a_+ and a_- are the respective ionic radii of the positive and negative species (Israelachvili 1992).

While solubility in itself is an equilibrium event, experimentally determined solubilities can produce different values for the same substance depending on the starting solid form and the measurement procedure (Sugano *et al.* 2007). The term solubility generally refers to thermodynamic equilibrium solubility, which is the solubility of the most stable crystal form in a specific environment (Kerns & Di 2008; Sugano *et al.* 2007; Bhattachar *et al.* 2006). For this equilibrium to be established, incubation times of several hours to days are generally required (Alsenz & Kansy 2007; Sugano *et al.* 2007).

Apparent solubility, on the other hand, signifies the solubility of a metastable or unstable solid form (Sugano *et al.* 2007; Bhattachar *et al.* 2006). Such apparent equilibria can occur in experiments where the starting material is a cocrystal, solvate, salt or meta-/unstable form, and the incubation times are not long enough to achieve crystal formation and equilibration with the most stable crystal polymorph (Sugano *et al.* 2007; Alsenz & Kansy 2007; Huang & Tong 2004). All unstable and metastable solid forms will eventually recrystallize to the most stable crystal form, and thus the solid form with the lowest solubility (Bhattachar *et al.* 2006). The apparent solubility is, therefore, always a case of sustained supersaturation.

A special case of apparent solubility is the kinetic solubility. The kinetic solubility is a measure of precipitation tendency, often in cosolvent systems (Sugano *et al.* 2007; Alsenz & Kansy 2007; Lipinski *et al.* 1997). The starting material in these measurements is dissolved material and the onset of precipitation, when adding to an antisolvent, is assumed as the solubility. According to the Ostwald 'rule of stages', the precipitate formed in such a process is often amorphous or a metastable polymorph and will therefore significantly overestimate the equilibrium solubility (Ostwald 1897).

For electrolytes, two further special cases of solubility exist, *i.e.* the native (S_N) and the intrinsic solubility (S_0). The native solubility is the solubility of an ionizable compound measured under unbuffered conditions. The final equilibrium *pH* in such measurements may vary significantly from the initial *pH* due to self-buffering effects (Serajuddin & Jarowski 1985). The intrinsic solubility again, is the solubility of the unionized form of an electrolyte under buffered conditions (Sugano *et al.* 2007). For ionizable molecules the intrinsic solubility is thus measured at a *pH*, where the molecule does not dissociate. Through the Henderson-Hasselbalch equations (Eqs. 3 and 4) the relationship between equilibrium solubility, intrinsic solubility, pK_a and *pH* can be expressed as,

$$S = S_0(10^{pH-pK_a} + 1) \tag{8}$$

for an acid and,

$$S = S_0(10^{pK_a-pH} + 1) \tag{9}$$

for a base (Avdeef 2001). It can be appreciated from Equations 8 and 9 that the solubility of an ionizable compound increases exponentially with the difference between *pH* and pK_a.

2.1.3 Lipophilicity

The third thermodynamic equilibrium reviewed in this section is the partition coefficient *P* (often given in the logarithmic form as *logP*), which describes the partitioning of an undissociated or neutral molecule between two immiscible phases. This partitioning is also determined by the energy difference between molecules in the two phases, and is expressed by the Boltzmann distribution (Eq. 2) as,

$$X_2 = X_1 exp\left[\frac{-A(\gamma_{BC}-\gamma_{AC})}{k_B T}\right] \tag{10}$$

where A is the solvent exposed surface area of a molecule or particle ($4\pi r^2$ for a sphere) and γ_{BC} and γ_{AC} are the interfacial energies between the respective solvent-particle interfaces (Israelachvili 1992).

The partition coefficient is often measured between an organic octanol phase and an aqueous phase. The *logP* can be expressed in a simplified form as the concentration difference between these two phases,

$$logP_{oct/w} = \frac{[HA_{oct}]}{[HA_w]} = \frac{S_{oct}}{S_w} \tag{11}$$

where S_{oct} is the equilibrium solubility in octanol and $S_W = S_0$ in the case of electrolytes (Jain & Yalkowsky 2001). As in the case of the GSE, the interrelationship between lipophilicity and solubility is again demonstrated by the fact that the *logP* can be expressed in terms of solubility of a substance in the respective solvent. A higher *logP* will therefore be generally associated with lower aqueous solubility. It can be noted that one of the original aims of *logP* measurements was to find a descriptor that would mimic the partitioning of a molecule between an aqueous phase and a cell membrane (Waring 2010).

For electrolytes, the effect of pK_a of the molecule and *pH* of the solvent have to be taken into consideration once more and the logarithm of the distribution coefficient (*D*) can be expressed in a simplified form as,

$$logD_{oct/w} = logP + log\left[\frac{1}{1+10^{pH-pK_a}}\right] \tag{12}$$

for acids and,

$$logD_{oct/w} = logP + log\left[\frac{1}{1+10^{pK_a-pH}}\right] \tag{13}$$

for bases (Scherrer & Howard 1977). The distribution coefficient is always represented with the *pH* at which it was acquired, and describes the ratio of the concentration of the undissociated molecule in the organic phase to the concentration of all species in the aqueous phase. For neutral compounds *logP* equals *logD*, but for electrolytes *logP* will be higher than *logD* at *pH* values where the electrolyte dissociates, as the charged species will partition into the aqueous phase.

2.1.4 Dissolution rate

In contrast to the equilibrium constants presented in the previous sections, the rate of dissolution is a kinetic process determined by several equilibria. The dissolution of a solid in a liquid involves two steps: overcoming the cohesive forces of the solid phase, by the energetic interaction between solute and solvent molecules at the solid-liquid interface; and the subsequent diffusion of the dissociated molecules into the bulk solvent. It is thus the difference in energy between the intermolecular solid-solid and liquid-liquid interactions and the subsequently formed solid-liquid interactions that determine the overall dissolution rate (Israelachvili 1992; Yalkowsky & Valvani 1980).

The three physical models that are commonly used to describe the dissolution of a pure solid substance in a homogeneous solvent are the diffusion layer model (Nernst 1904; Bruner & Tolloczko 1901; Noyes & Whitney 1897), the interfacial barrier model (Wurster & Taylor 1965) and Dankwerts' surface renewal model (Danckwerts 1951). Of these the diffusion layer model has become the most prominently used (Dejmek & Ward 1998; Wurster & Taylor 1965).

According to the diffusion layer model, a diffusion layer of thickness (h) is formed at the solid-liquid interface (Higuchi 1967; Nernst 1904; Noyes & Whitney 1897). Inside this diffusion layer a rate limiting concentration gradient is assumed, ranging from saturation concentration (S) at the solid-liquid interface (h=0) to the homogenous bulk concentration (C_t) outside the diffusion layer. The diffusion layer assumption arises from another assumption, that the interfacial reaction rate is much faster than the Brownian diffusion or convective rate of transport into the solvent (Wurster & Taylor 1965).

The classical Noyes-Whitney equation was the first to express the diffusion layer theory in quantitative terms,

$$\frac{dC}{dt} = k(S - C_t) \tag{14}$$

where dC/dt expresses the change in bulk concentration with time (t) and,

$$k = \frac{D_c A}{Vh} \tag{15}$$

where D_c is the diffusion coefficient within the layer, V is the volume of the solvent and h is the thickness of the diffusion layer (Nernst 1904; Bruner & Tolloczko 1901; Noyes & Whitney 1897). The similarity of the diffusion rate model with Fick's laws of diffusion is apparent (Fick 1855).

The diffusion coefficient for a spherical particle has been theoretically derived with the Stokes-Einstein equation (Einstein 1905), however, it can also be approximated from a simplified semiempirical version of the equation,

$$D_c = \frac{2.40\times10^{-3}}{MW^{1/3}} \tag{16}$$

(Al-janabi 1990). The diffusion layer thickness, on the other hand, has been estimated to be approximately 30 μm, for particles with a radius significantly above 30 μm and to decrease proportionally with the particle radius below this threshold (Hintz & Johnson 1989).

The diffusion layer theory has subsequently been modified to model the dissolution of single spherical particles (Niebergall *et al.* 1963; Higuchi & Hiestand 1963; Hixson & Crowell

$${M_t}^x = M_0^x - k_x t \tag{17}$$

where M_t is the mass of the dissolving particle at time t, M_0 is the initial mass of the dissolving particle and k_x is a model specific rate constant, three single-particle models can be derived by substituting the exponent (x) with ⅓, ½ or ⅔ (Wang & Flanagan 1999). The cube root expression is called the Hixson-Crowell cube root law,

$$Kt = M_0^{1/3} - M_t^{1/3} \tag{18}$$

and

$$K = \frac{\left(\frac{4\pi\rho}{3}\right)^{1/3} D_C S}{\rho h} \tag{19}$$

where ρ is the density of the particle (Wang & Flanagan 1999; Hixson & Crowell 1931). The Hixson-Crowell cube root law is the most appropriate of the single-particle expressions to model the dissolution of particles larger than the diffusion layer thickness (*i.e.* 30 µm). It was derived assuming a changing surface area under the special case of sink conditions $S \ll C_t$, *i.e.* in an environment where the dissolved fraction does not affect the dissolution rate and, thus, Equation 14 from the perspective of the dissolving particle becomes,

$$\frac{dM}{dt} = kAS \tag{20}$$

where dM/dt expresses the change in mass of the particle with time. The rate of dissolution per surface area and time, measured under sink conditions, is called the intrinsic dissolution rate (IDR),

$$\frac{dM}{Adt} = \frac{D_C}{h} S \tag{21}$$

(Serajuddin & Jarowski 1985; Levich 1962). It should be noted that due to possible self-buffering activity of ionizable compounds, the rate limiting solubility factor in Equations 14 and 19 to 21, will be the solubility of the dissolving substance at the *pH* of a saturated solution (Serajuddin & Jarowski 1985).

It can be observed from the preceding section, that solubility and thus lipophilicity and charge state are intimately related with the dissolution rate (Eqs. 14, 19 to 21). As stated in the beginning of the chapter, one has to bear in mind that the equations presented herein are often only approximate and do not remove the need for accurate experimental measurements. This becomes especially true under complex physiological conditions, which cannot be accurately modeled by simple two phase equilibria. For example, factors such as effects of the formulation, excipients, temperature, ionic strength, surface active agents and the mean intestinal transit time (MITT) all come into play for drug products during *in vitro* experiments, and further after *in vivo* administration orally into the gastrointestinal (GI) tract or by other routes (Dressman *et al.* 1998).

2.2 Physicochemical parameters in pharmaceutical research

Key physicochemical properties determining the developability and biological activity of compounds include pK_a, solubility, dissolution rate, lipophilicity, permeation (P), stability, *MW*, polar surface area (PSA), number of hydrogen bond donors (HBD) or acceptors (HBA) and the number of rotatable bonds (NROT) (Waring 2010; Alsenz & Kansy 2007; Kerns 2001; Lipinski *et al.* 1997). These substance characteristics have been combined in different 'rules' and frameworks in order to categorize molecules and describe their lead- or drug-likeness. Some examples include Lipinski's rule of five, the rule of three, lipophilic ligand efficiency

(LLE), ligand-efficiency-dependent lipophilicity (LELP), the 3/75 rule, Veber's criteria and the biopharmaceutics classification system (BCS) (specifics are found in Table 1) (Keserü & Makara 2009; Hughes *et al.* 2008; Leeson & Springthorpe 2007; Congreve *et al.* 2003; Veber *et al.* 2002; Lipinski *et al.* 1997; Amidon *et al.* 1995).

Table 1. Lead-/drug-likeness, developability criteria and the biopharmaceutics classification system (BCS)

Rule of five[1]	HBD <5, HBA <10, MW <500, logP <5	**BCS II** Low S, High P	**BCS I** High S, High P
Rule of three[2]	HBD ≤3, HBA≤3, MW <300, logP ≤3		
LLE[3]	logP/ligand efficiency (0-7.5)		
LELP[4]	pIC_{50} (or pK_i) – logP (or logD) >5-7	**BCS IV** Low S, Low P	**BCS III** High S, Low P
3/75 rule[5]	logP <3, PSA >75 Å2, if C_{max} <10 μm		
Veber's criteria[6]	PSA ≤140 $Å^2$ (or HBD+HBA ≤12), NROT ≤10		

[1](Lipinski *et al.* 1997), [2](Congreve *et al.* 2003), [3](Leeson & Springthorpe 2007), [4](Keserü & Makara 2009), [5](Hughes *et al.* 2008), [6](Veber *et al.* 2002). H-bond donor (HBD), H-bond acceptor (HBA), molecular weight (MW), partition coefficient (P), distribution coefficient (D), half maximal inhibitory concentration (IC_{50}), inhibition constant (K_i), polar surface area (PSA), peak serum concentration (C_{max}), number of rotatable bonds (NROT), solubility (S), permeability (P).

The main aim of such characterization is to identify the most promising compounds and solid forms that will achieve a therapeutic and non-toxic profile *in vivo,* by the intended route of administration (Alsenz & Kansy 2007; Leeson & Springthorpe 2007; Gardner *et al.* 2004). It is evident that the earlier high quality parameters can be achieved, the faster the decision-making and, consequently, the whole drug development process will be. Many of the aforementioned parameters can be acquired from *in silico* data, whereas permeation and stability measurements require more advanced methods. Solubility, dissolution rate, lipophilicity and pK_a, which are fundamental throughout pharmaceutical research can, on the other hand, be experimentally acquired by relatively simple *in vitro* techniques.

Solubility, dissolution rate, pK_a and lipophilicity profoundly influence the PK of a compound (Figure 1) (Waring 2010; Tong *et al.* 2009). These parameters are also determinants of pharmacological efficacy, as only a dissolved molecule remaining in solution at the site of action will elicit any therapeutic response (Morgan *et al.* 2012; Gleeson 2008). As stated by Curatolo: "An efficacious but nonabsorbed agent is no better than a well-absorbed but inefficacious one" (Curatolo 1998). Data of these properties are important input parameters for *in silico* prediction software and are used in the preclinical discovery phase to establish quantitative structure activity (QSAR) and quantitative structure property relationships (QSPR) (Tong *et al.* 2009; Alsenz & Kansy 2007; Gardner *et al.* 2004; Kerns 2001).

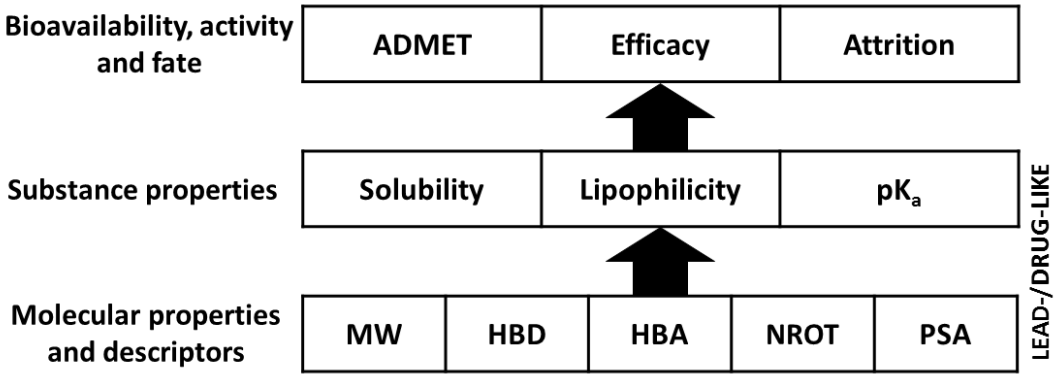

Figure 1. Physicochemical properties of substances and impact. Molecular properties determine substance properties, which in turn determine the bioavailability, biological activity, efficacy and fate of a drug in the development process. Absorption, distribution, metabolism, excretion and toxicity (ADMET), ionization constant (pK_a), molecular weight (MW), H-bond donor (HBD), H-bond acceptor (HBA), number of rotatable bonds (NROT), polar surface area (PSA).

With up to 75% of current drug candidates demonstrating low aqueous solubility, the importance of solubility assessment as a predictive tool for *in vivo* drug biological activity is increasing (Di *et al.* 2009). Solubility in various media including aqueous buffers, organic solvents, formulation vehicles and simulated or native biological fluids is assessed in order to assist in synthesis and solid form optimization, administration route selection, formulation strategies for animal toxicology and clinical studies, processability assessment and to indicate potential PK liabilities of the compounds (Alsenz & Kansy 2007; Gardner *et al.* 2004; Kerns 2001; Merkle & Jen 2002). Dissolution rate is assessed in particular for poorly soluble active pharmaceutical ingredients (APIs) of BCS classes II and IV intended for oral administration (Tong *et al.* 2009; Alsenz & Kansy 2007). Especially the dissolution rate and apparent solubility can be enhanced through chemical structure, salt and solid form modifications (Sugano *et al.* 2007; Faller & Ertl 2007; Huang & Tong 2004).

The lipophilicity of a molecule, on the other hand, greatly influences all ADME parameters. The most obvious connection is with aqueous solubility, with increased lipophilicity resulting in a decrease in aqueous solubility (Waring 2010; Gleeson 2008). High lipophilicity is also related to increased metabolism through higher binding affinity with drug-metabolizing cytochrome P450 enzymes (Gleeson 2008; Lewis & Dickins 2003). Low lipophilicity, on the other hand, has been linked to bioavailability issues through an increase in renal clearance and decrease in biological membrane, *e.g.* intestinal or blood-brain barrier, permeation (Waring 2010; Gleeson 2008). The link between lipophilicity and *in vitro* cellular permeability on *in vivo* absorption has been thoroughly established (Waring 2010; Linnankoski *et al.* 2006; Winiwarter *et al.* 1998; Lipinski *et al.* 1997). Furthermore, lipophilicity has been found to be a major determinant in the degree of plasma protein and tissue binding, as well as the distribution in the body and on a cellular level (Gleeson 2008; Valko *et al.* 2003; Gerweck *et al.* 1999). Studies have also found a difference between the degree of lipophilicity of drugs between target protein classes and therapy areas (Waring *et al.* 2015; Leeson & Springthorpe 2007; Morphy 2006). The charge state of a molecule, determined by the pK_a, plays a complex role in all of these processes. It is generally acknowledged that a molecule will dissolve more readily in the ionized form, while a molecule predominantly permeates cellular membranes in the neutral form (Waring 2010). The effect of charge state

on other ADME parameters is more intricate and not equally well understood (Gleeson 2008). Obviously, all of the aforementioned physicochemical characteristics will continue to affect the distribution and accumulation of substances also in the environment after being eliminated (Bangkedphol *et al.* 2009).

As a consequence of the introduction of HTS and combinatorial chemistry for identifying potent hits, the trend in drug development candidates has shifted toward poorer physicochemical properties including high lipophilicity and poor aqueous solubility (Alsenz & Kansy 2007; Leeson & Springthorpe 2007; Gardner *et al.* 2004). Such issues of inadequate physicochemical properties of candidate molecules can lead to more challenging development programs and time-consuming iterations in the R&D process (Waring *et al.* 2015; Leeson & Springthorpe 2007; Kola & Landis 2004; Gardner *et al.* 2004). However, concurrently the attrition of NMEs directly caused by inadequate PK and bioavailability issues has decreased significantly during the last two decades, currently accounting for some 10% of all attrition (Waring *et al.* 2015; Kola & Landis 2004).

The two major causes of attrition today are inadequate safety and efficacy (Waring *et al.* 2015; Cook *et al.* 2014; Kola & Landis 2004). The indirect effect of poor physicochemical properties of compounds behind these main causes could, however, be substantial, and the importance of thorough physicochemical characterization has lately, once again, been brought into focus (Waring *et al.* 2015; Morgan *et al.* 2012; Gleeson 2008; Leeson & Springthorpe 2007; Di & Kerns 2006).

While solubility is mainly assessed in the framework of PK it also plays an intricate role in many processes including biological assays (Di & Kerns 2006; Gardner *et al.* 2004). This is because insufficient solubilization and potential precipitation and aggregation of a compound under storage and biological assay conditions can lead to erroneous estimations of compound activity (Di & Kerns 2006). For example the reduced concentration of insoluble compounds in a HTS assay, led to a hit rate of 4%, while compounds of higher solubility showed a hit rate of 32% (Popa-Burke *et al.* 2004). As poor aqueous solubility of lead molecules has become a major issue, up to 30% of lead compounds could have their activity wrongly estimated in ADME and toxicology (ADMET) assays due to an inability to reach sufficient concentrations (Di *et al.* 2009; Lipinski 2001). The importance of knowing the solubility of development compounds in different environments is thus highlighted (Di & Kerns 2006). Furthermore, co-solvents such as dimethyl sulfoxide (DMSO) can interfere with enzyme and cell assays, leading to discrepancies in the data (Di & Kerns 2006). It is obvious that false data will lead to inaccurate QSAR modeling, problems with false or missed leads and unnecessary iterations downstream in the R&D process (Di & Kerns 2006; Gardner *et al.* 2004). It would therefore be important to screen solubility under assay conditions before initiating biological activity screens (Alsenz & Kansy 2007). Going further, an inability to achieve meaningful plasma levels in preclinical animal studies, due to poor solubility and insufficient dissolution, can mask underlying toxicity and metabolic issues that will appear only at a later, more costly stage in the development process (Gardner *et al.* 2004).

High lipophilicity is, on the other hand, strongly correlated with increased risk for pharmacological promiscuity, *i.e.* the binding to multiple targets, one of the causes of toxicology attrition (Waring *et al.* 2015; Leeson & Springthorpe 2007). Lipophilicity is also strongly connected with two other causes of specific toxicity common for drugs: the binding affinity to the cardiac hERG potassium channel and drug induced phospholipidosis (Waring & Johnstone 2007; Tomizawa *et al.* 2006; Ploemen *et al.* 2004). Such 'off-target' toxicological events have been found to contribute to up to 75% of preclinical safety attrition (Cook *et al.* 2014). A narrow range of *logD* between 1 and 3 has been identified as the optimal range to

avoid developability and toxicology issues while maintaining sufficient potency (Waring 2010). For example compounds with a calculated l*ogP* above 3 were found to be 2.5 times more toxic than compounds within the optimal range in *in vivo* animal studies (Hughes *et al.* 2008).

The relationship between increased lipophilicity and increased risk of attrition in clinical safety studies has also been demonstrated (Waring *et al.* 2015). A statistically significant decrease in calculated *logP* and $logD_{7.4}$ values has been observed for drug candidates progressing into later stage clinical development phases, with launched drugs having the lowest lipophilicities (Waring *et al.* 2015; Wenlock *et al.* 2003). This suggests a direct effect of higher lipophilicity on compound attrition in both discovery and development. Efficacy issues can, on the other hand, arise due to limitations in the dose or inability to achieve sufficient exposure in the target tissue (Cook *et al.* 2014). As previously discussed, these issues can be related to physicochemical characteristics of the compounds, and account for some 30% of efficacy related attrition.

As has been discussed, the direct and indirect effects of drug physicochemical properties are paramount during the whole R&D process. There is evidence that both poor solubility and high lipophilicity increases the risk of developability and safety issues, as well as compound attrition (Alsenz & Kansy 2007; Leeson & Springthorpe 2007). Recently, a shift toward a more holistic approach in compound selection and optimization has been indicated, with an aim to achieve increased potency while simultaneously maintaining optimal physicochemical characteristics of the drugs (Leeson & Springthorpe 2007; Gardner *et al.* 2004). The incentive surely exists as only a 5% improvement in attrition would result in a twofold increase in the output of new drugs (Leeson & Springthorpe 2007). In order to achieve this, high quality procedures and technologies are required, from the earliest stages of the R&D process.

2.3 Physicochemical characterization methods

It has been estimated that up to 10^{24} different drug compounds could be synthesized by modern combinatorial chemistry (Ertl 2003). The vast amount of molecules being screened by HTS for potency and the practically infinite chemical space represented by these possible drug molecules, poses a real challenge for analytical methods in preclinical R&D. Another issue for early physicochemical property assessment is the low amounts (less than a few milligrams) of available compound for physical *in vitro* screening at this stage (Lipinski *et al.* 1997; Sugano *et al.* 2007; Kerns 2001). At later stages in the development process, where larger batches of higher purity of the most promising candidates are synthesized, the need for rapid characterization methods persists as the number of screened solvents increases markedly (Alsenz & Kansy 2007). In light of this, a set of optimal requirements for high throughput physicochemical profiling methods has been proposed (Gardner *et al.* 2004; Kerns 2001):

- Throughput of >50 compounds/instrument/day;
- Low total substance consumption (mg);
- Non-specific methods for coverage of wide chemical space;
- Quality information relevant for decision-making;
- Automation of sample preparation, measurement and analysis.

In summary, the challenge lies in decreasing resource and time consumption, while simultaneously maintaining the quality of the aquired data.

2.3.1 In silico methods

Due to the lack of experimental methods capable of accommodating the requirements for throughput and low materials consumption, computational methods are used in early discovery (Tetko *et al.* 2009; Gardner *et al.* 2004). However, these *in silico* methods are also challenged by the vast dimensionality of the possible chemical space of drug molecules (Tetko *et al.* 2009).

In silico models are inherently limited to their applicability domain, *i.e.* to the chemical space of the training set used to validate a method (Tetko *et al.* 2009; Mannhold *et al.* 2009; Faller & Ertl 2007). Despite considerable efforts to develop accurate *in silico* methods for solubility, lipophilicity and pK_a prediction, the lowest achievable root mean square errors (RMSE) of predictions within the applicability domains generally remain around 0.8 log units (Balogh *et al.* 2012; Tetko *et al.* 2009; Mannhold *et al.* 2009; Jorgensen & Duffy 2002). Outside this domain the prediction errors can be as high as 1 to 3 log units and a general arithmetic average model, where the average value of the training set is attributed to all molecules, often succeeds better than an actual prediction.

Moreover, *in silico* models are validated by their comparison with experimental values. Consequently, one of the reasons for the poor predictivity, even within the applicability domains of the models, has been attributed to the lack of high quality homogeneous datasets of experimental values, commonly referred to as 'garbage in garbage out' (Di *et al.* 2012; Tetko *et al.* 2009; Faller & Ertl 2007; Linnankoski *et al.* 2006). Furthermore, the experimental input parameters used in validation studies have to be acquired under a potentially large range of relevant chemical conditions reflecting the model environment (Bangkedphol *et al.* 2009; Sugano *et al.* 2007). It is therefore generally believed that the accessibility of accurate high-quality experimental datasets would improve prediction accuracy by minimizing the systematic errors introduced through poor input parameters (Tetko *et al.* 2009).

As first introduced by Hansch (Hansch *et al.* 1968), most *in silico* methods for solubility prediction, *e.g.* the GSE (Eq. 6), are based on the relationship between *logP* and S_o. Due to the lack of high-quality experimental datasets, calculated *logP* values in combination with a variation of molecular descriptors, such as the PSA, are generally used (Faller & Ertl 2007). It is evident that the predictive power of solubility models will be limited by the inherent error of the underlying calculated *logP* values, in addition to the errors of the actual solubility model. In the case of solubility, lattice energies and crystal packing calculations, in particular, require expensive computations and are difficult to predict (Faller & Ertl 2007). Furthermore, most *in silico* models are only applicable for predicting *logP* and water solubility of neutral and undissociated molecules, and are often confined to the parent moiety (*i.e.* not salts or solvates) (Gardner *et al.* 2004). Some methods have been developed for solubility in DMSO, surfactants and cosolvent solutions, but most models do not consider the complex composition of GI fluids (Alsenz & Kansy 2007; Gardner *et al.* 2004). In case of ionizable molecules the accuracy of the *logD* and solubility predictions will further depend on the calculated pK_a value (see Eqs. 8, 9, 12 and 13). These uncertainties need to be taken into account in decision-making as well as in the analysis of, for instance, lipophilicity and solubility dependent attrition (Waring 2010).

2.3.2 In vitro methods

It is evident from the foregoing section, that *in silico* predictions have not diminished the need for high-quality and HTE methods in pharmaceutical research. In this section some of the most used miniaturized experimental methods will be reviewed.

2.3.2.1 Dissolution rate

The kinetic nature of dissolution could reflect *in vivo* events in more detail than solubility, as dissolution rate data incorporates the initial wetting stage, the impact of diffusion as well as the effect of solid state properties (Zakeri-Milani *et al.* 2009; Yu *et al.* 2004). Thus, earlier acquisition of dissolution rate data would provide high quality input parameters for early stage ADMET models (Alsenz & Kansy 2007). Especially the intrinsic dissolution rate could be suitable for high-throughput screening applications, since data from only the first 10% of the dissolution curve is usually required for determination (USP 2015). Moreover, due to the higher *in vivo* relevance of dissolution rate data, it has been proposed that IDR, rather than solubility, should be the basis of the biopharmaceutical classification of drugs (Table 1) (Yu *et al.* 2004).

Despite these apparent advantages, small scale dissolution methods are scarce and miniaturization is often based on the well-known compendial apparatus (USP 2015; Klein & Shah 2008). The method most often used as a comparison in these measurements is the disc-IDR (DIDR). One miniaturized version of the DIDR apparatus, the Mini-IDR method, has shown good correlation with DIDR data, and the substance consumption in this method has been reduced to as little as 5 mg per experiment (Avdeef 2008).

Non-traditional methods have also been presented. One variation is a flow-through setup using detection by UV imaging and requiring sample amounts of 3-10 mg per experiment (Østergaard *et al.* 2014; Hulse *et al.* 2012). Another, the powder-IDR (PIDR) method introduced by Tsinman and coworkers (2009), has produced comparable data with the standard DIDR method, using powder samples as small as 60 µg and *in situ* fiber-optic UV analysis. The disadvantage of powder based approaches lies in the lack of understanding and the difficulty of modeling multiparticle systems, leading to rough estimations (Hulse *et al.* 2012; Avdeef *et al.* 2009; Wang & Flanagan 1999; Mosharraf & Nyström 1995). Small particles have larger surface energies, due to the increased surface curvature, increasing the probability of particle aggregation and agglomeration (Yu 1999; Wang & Flanagan 1999). The dissolution rate of multiparticle systems is therefore an expression of the dissolution from the mean effective surface area, determined by the particle size distribution and the extent of aggregation and agglomeration in the system (de Villiers 1996). The difficulty is further increased by the dynamic change of these factors during the dissolution process.

The drawback of the Mini-IDR and flow cell methods is the relatively high substance consumption and the need for sample preparation, often into a compact of known surface area (Hulse *et al.* 2012; Avdeef 2008). In addition, all the methods have relatively low throughput and are based on specific UV detection, thus increasing the use of substance through detection range scanning and calibration.

2.3.2.2 Solubility, lipophilicity and pK_a

'Gold standard' shake-flask method

The 'gold standard' method for solubility and lipophilicity assessment is the classical thermodynamic shake-flask method (OECD 2016a; OECD 2016b ; Kerns 2001; Danielsson & Zhang 1996; Dittert *et al.* 1964). For thermodynamic solubility to be determined, an excess amount of solid is brought in contact with the solvent, and the equilibrium concentration is determined after long incubation times, usually in the range of several hours to days (Alsenz & Kansy 2007; Sugano *et al.* 2007; Lipinski *et al.* 1997). For lipophilicity measurements, a similar shaking and phase separation timeframe is required (Danielsson & Zhang 1996). The amounts required per experiment are generally in the mg and g range and quantitation requires substance specific chemical analysis, after separation of solid from the liquid or of the two liquid phases. Consequently, accurate determination of equilibrium solubility and lipophilicity by traditional means is both time and substance consuming.

While thermodynamic solubility is often regarded as the 'true' solubility, the measured values are not absolute and depend on both compound properties and experimental factors (Alsenz & Kansy 2007). Such factors can be related to weighing, adsorption and absorption to materials during liquid sample handling, such as filtration, centrifugation and pipetting and further to analytical discrepancies. In fact, the range of uncertainty of thermodynamic solubility values reported in literature has been shown to be in the range of 0.6 log units (Jorgensen & Duffy 2002; Katritzky *et al.* 1998).

Miniaturized versions of the shake-flask method, some 96-well plate based, have been developed for both solubility and lipophilicity studies (Heikkilä *et al.* 2011; Glomme *et al.* 2005; Bergström *et al.* 2004; Kerns 2001). While the substance consumption in these methods has been substantially decreased to around 1 mg, the time scale of the measurements is still comparable to that of the shake-flask method, *i.e.* several hours and usually up to 24 h. High-throughput applicability of thermodynamic solubility measurements is therefore not yet possible.

Potentiometric methods

For pK_a measurement, the classical method is potentiometric acid-base titration (Comer 2003; Kerns 2001). In this method, the *pH* is measured continuously during acid or base titrant addition and the difference spectrum between a pure water blank run and a run with the dissolved compound gives the pK_a (Slater *et al.* 1994). As the compound has to be dissolved in pK_a measurements, it is often challenging to acquire quantifiable concentrations for poorly soluble compounds (Takács-Novák *et al.* 1997). In such cases organic cosolvents can be used, and the results from different ratios of the organic and aqueous phases extrapolated to pure aqueous phase, with good correlation. One automated aqueous titration usually requires 10-30 min, but with cosolvent systems the amount of runs will obviously be manyfold (Slater *et al.* 1994).

Potentiometric analysis can also be used for *logP* measurement of ionizable molecules (Slater *et al.* 1994). In this case, *logP* is calculated from the shift in pK_a, called apparent pK_a, caused by partitioning of the neutral species into the octanol phase. The time required for such runs is generally 20-60 min. Further, potentiometry can be used to determine aqueous solubilities of ionizable molecules (Avdeef 1998). During potentiometric solubility

measurement, the titration starts from a *pH* at which the molecule is fully ionized and dissolved (Avdeef 1998). As the titration progresses, precipitation occurs in the range of the pK_a of the molecule. Analogous to the case of *logP* measurement, an apparent pK_a shift occurs due to precipitation of the poorly soluble neutral species. Solubility is then calculated based on the difference between the apparent pK_a and the known true pK_a of the substance. The method has been shown to produce comparable results with the 'golden standard' shake-flask method (Glomme *et al.* 2005; Avdeef *et al.* 2000). Approximately 100 µg of substance is required per run and produces a full pH-solubility profile (Glomme *et al.* 2005; Avdeef & Berger 2001). The time required for a potentiometric titration depends on the solubility of the compound as well as the solvents used. One run generally requires 3-36 h and a throughput of three poorly soluble substances per week has been estimated (Stuart & Box 2005; Glomme *et al.* 2005).

A simplified version of the potentiometric method called 'chasing equilibrium' has been introduced for more rapid assessment of intrinsic solubility of ionizable compounds (Stuart & Box 2005). In this procedure, the intrinsic solubility equilibrium is actively sought, by addition of acid or base titrant, to alternately dissolve and precipitate the sample. Monitoring the change in *pH* during the process enables the determination of the *pH* at which the rates of precipitation and dissolution are equal. Intrinsic solubility measurement using this method requires typically between 20-80 min and the lower limit for the required amount of sample is around 2-5 mg, with an average of around 60 mg per measurement.

A prerequisite for potentiometric determination of solubility and lipophilicity is an accurate value for the pK_a(s) of the molecule, with the estimation error between *e.g.* pK_a and $\log S_o$ being directly proportional. While the potentiometric solubility method produces a full *pH*-solubility profile, from as little as 100 µg of sample, the throughput of the method brings no real advantage in time compared to the shake-flask method. The 'chasing equilibrium' method, on the other hand is substantially faster, but requires comparably large amounts of substance. It is apparent from the timescales of the potentiometric pK_a, lipophilicity and solubility measurements that high-throughput applicability of the method is not yet possible. However, the greatest disadvantage of potentiometric solubility measurement is that it is limited to ionizable molecules.

Chromatographic and gradient analysis methods

Reversed phase high-performance liquid chromatography (HPLC), capillary electrophoresis (CE) and spectral gradient analysis (SGA) have also been applied to determine pK_a and lipophilicity of compounds (Cabot *et al.* 2015; Box *et al.* 2003; Lombardo *et al.* 2000; Poole *et al.* 2000; Valkó 1997). These methods require very small liquid sample amounts (µL range) and are applicable in high-throughput studies, with quantitation usually based on UV or mass spectrometry (MS). In reversed phase HPLC and CE, the movement of a molecule through a column depends on the partitioning between a stationary organic phase and a moving aqueous phase, or on the different electrophoretic mobility of neutral and ionized species (Cabot *et al.* 2015; Lombardo *et al.* 2000; Poole *et al.* 2000; Valkó 1997). SGA, on the other hand, is based on injecting samples into a linearly changing *pH* gradient flow, and detecting the change in UV absorbance of a chromophore near to the ionization center of the dissociating molecule (Box *et al.* 2003).

Kinetic solubility

For high-throughput solubility measurement, the currently most used method in preclinical drug discovery is the kinetic solubility method (Alsenz & Kansy 2007). Kinetic solubility is determined starting from dissolved compound, usually DMSO stock solutions, as the time point preceding precipitation in a dilution series into aqueous buffer (Alsenz & Kansy 2007; Lipinski *et al.* 1997; Bevan & Lloyd 2000). In the turbidimetric method, an amount of DMSO stock solution of known concentration is added at the rate of 1 mL/min into a cuvette containing *pH* 7 phosphate buffer (Lipinski *et al.* 1997). Precipitates are detected in a UV spectrophotometer from the absorbance increase of the turbid solution. The nephelometric method, on the other hand, uses serial dilution of the stock solution of known concentration into a 96-well plate (Bevan & Lloyd 2000). The plate is scanned by a laser nephelometer and the scattered light at a right angle is measured.

Kinetic solubility measurement is the only solubility method currently achieving high-throughput, with a capability of analyzing 50-300 samples per day (Glomme *et al.* 2005). Another advantage of the method is the use of DMSO stock solutions, which are readily available from HTS assays. Moreover, methods based on light scattering are non-specific and applicable to all substances and transparent solvents as such.

However, kinetic solubility values have been shown to be poor predictors of equilibrium solubility, with estimation errors up to 1.7 log units (Lipinski *et al.* 1997; Stuart & Box 2005). The uncertainty arises from several sources. The presence of DMSO in the solution, in addition to the short incubation times, often leads to supersaturation by solubilization and precipitation of an unstable or a metastable form in accordance with the 'Ostwald rule of stages' (Sugano *et al.* 2007; Alsenz & Kansy 2007; Kerns 2001; Ostwald 1897). Furthermore, the act of predissolving in DMSO masks the influence of crystal lattice energies and polymorphic forms on solubility, and consequently, the data is not applicable as an input parameter for QSPR assessment (Huang & Tong 2004; Lipinski *et al.* 1997). As the measurement error is in the range of *in silico* prediction uncertainty (as previously reviewed), the question can be raised if such experimental values provide any additional value to the research scientist.

Based on this review of current state of the art methods for physicochemical analysis, it is evident that no one method is capable of accurate assessing all of solubility, lipophilicity and pK_a. For solubility measurement in particular, there appears to be a discrepancy between throughput, substance consumption and accuracy. High-throughput invariably leads to higher substance consumption, or conversely a decrease in accuracy. High accuracy on the other hand requires slow measurements or higher amounts of substance. In order to achieve a unity between these aspects, novel approaches are needed.

2.4 Microscopy and single-particle analysis

The development, implementation and validation of an analytical method can often be the most time-consuming step of an experimental process (Glomme *et al.* 2005). One weakness of commonly used chemical analysis techniques is the extensive sample preparation, which includes both sample and calibrant preparation (Paakkunainen *et al.* 2009; Alsenz & Kansy 2007). The total measurement error of a method is, obviously, determined by the inherent error in every step of the procedure (Paakkunainen *et al.* 2009; Faller & Ertl 2007). This is especially true for miniaturized high-throughput measurements, where the relative error is

increased with decrease in sample size. While UV spectrophotometry is the most widely available chemical analytisis technique, the analysis of small and dilute samples often requires more sophisticated analytical methods, such as HPLC-MS or tandem mass spectrometry (HPLC-MS/MS) (Korfmacher 2005; Tiller *et al.* 2003). These methods are also the most used techniques for high-throughput quantitative analysis, with automated and optimized HPLC-MS methods achieving sample analysis times as low as 15 s per sample (Saunders 2004). The drawback of such advanced methods is, however, that the apparatus is expensive and costly to operate.

Due to the wide range of chemical space covered by drug molecules, different, often substance and solvent specific, analytical methods are required (Tiller *et al.* 2003; Sacher *et al.* 2001). For example, in an attempt to analyze 60 different pharmaceutical compounds with a minimum amount of either gas chromatography-MS or HPLC-MS/MS methods, 6 different methods were needed (Sacher *et al.* 2001). More non-specific methods such as potentiometry suffer from other limitations, such as being confined to ionizable molecules (as reviewed in section 2.3.2.2.). Particle based analysis such as turbidimetry, on the other hand, is truly non-specific, as it does not depend on the chemical properties of the studied molecules or solvents. Such methods could therefore be opportune for high-throughput requirements.

2.4.1 Image-based analysis

Particle characterization methods are widely used in pharmaceutical sciences where the accurate shape and size analysis is regarded as the 'gold standard' in understanding powders and particulate systems (Gamble *et al.* 2015; Allen 1990). Optical microscopy has been a widely used technique in such morphological characterization of particles, but only recently have advances in digital imaging, computing and image analysis software enabled the use of optical microscopy in automated real-time analysis (Gamble *et al.* 2015; Burggraeve *et al.* 2011; Almeida-Prieto *et al.* 2006; Allen 1990).

Optical microscopy is generally used to study particles in the size range of 3 μm – 150 μm, *i.e.* the typical size range of pharmaceutical powders (Gamble *et al.* 2015; Allen 1990). The traditional minimum resolution of optical microscopy is 0.8 μm, however, the rapid advancement of digital image processing has already enabled the surpassing of this limit, with modern advanced optical techniques achieving spatial resolutions below 100 nm (Cotte *et al.* 2013). Another limitation of traditional optical microscopy is the limited depth of field. For example, when moving from a magnification of 100x to 1000x, the depth of field changes from around 10 mm to approximately 0.5 mm (Allen 1990).

The typical method to capture and process data acquired by microscopy, is imaging and image analysis. Light from the analyzed object is detected by an image sensor, usually a charge coupled device (CCD) or a complementary metal–oxide–semiconductor (CMOS) sensor, which then translates the data into digital micrographs. A digital image is composed of multiple squares called picture elements or pixels. The spatial resolution of an image is thus determined by the amount of pixels per image area and it has been shown that around 50 pixels are needed for a reliable assessment of particle shape (Gamble *et al.* 2015; Kröner & Doménech Carbó 2013).

In order to facilitate analysis, color micrographs [red, green and blue (RGB) channels] are usually converted into grayscale (monochrome) (Allen 1990). The pixels of monochrome images are represented by a numerical value between 0 and 255. This value determines the grayscale shade, with 0 representing a black pixel and 255 a white pixel, depending on the

brightness and hue of the individual pixels of the original RGB micrograph. The micrograph is then usually further processed, by *e.g.* removing noise and background, improving contrast and defining a region of interest (ROI) for further analysis. A multitude of more or less advanced processing algorithms exist for both open source and commercial platforms. The processing usually ends in defining a grayscale threshold value, based on which all pixels with numerical values below the threshold get the value 0 (black) and all pixels with numerical values above the threshold get the value 255 (white). Through this thresholding process, a black and white binary image is produced, which can be further optimized for analysis, through *e.g.* smoothing, filling holes, defining edges and boundaries and segmenting regions. Image analysis can then be performed and object characteristics extracted.

In order to enable accurate 3D characterization of particle morphology, the particle generally has to be imaged from two or more defined or random angles (Frank *et al.* 1996; Podczeck 1995). As imaging is usually performed from only one direction, the orientation of the analyzed object determines the captured two-dimensional projection. For symmetrical objects such as spheres, that show the same two-dimensional projection in all directions, this is not an issue. 3D characteristics of non-spherical particles (*i.e.* volume and surface area), however, are usually based on equivalent sphere approximations. Therefore, a shape factor has to be applied to correct for the divergence from the ideal spherical shape. Several shape-factors, based on different ratios of the measured particles, have been developed through the years (Blott & Pye 2007). However, the assignment of shape factors to particle morphologies is non-trivial, and remains ambiguous and one of the most difficult particle characteristics to quantify (Blott & Pye 2007; Podczeck 1997).

2.4.2 Single-particle analysis

Despite these challenges, image-based microscopy could have great potential as an analytical method. The advantages of image analysis over other methods are as follows: non-specificity, straightforward automation, potential for very rapid data acquisition and real-time analysis, reduction of sampling steps and the avoidance of liquid sample handling, reduction of operator contact with potentially hazardous substances, as well as the possibility for reanalysis and visual inspection of possible causes of deviation in the acquired data.

Indeed, image-based microscopy has rapidly been gaining ground in biosciences, where it is used in *e.g.* high content analysis (HCA) of single cells, allowing the mining of large amounts of cell specific characteristics in a fast, robust and cost-effective manner (Marx 2012; Bakal *et al.* 2007). Further, the synergistic fusion of photonics and fluidics in smart diagnostic systems, so called optofluidic systems, has provided promising new applications for small-scale life science analytics (Schmidt & Hawkins 2011; Fan & White 2011). For example, optical and hydrodynamic single-cell manipulation and trapping has been widely used in miniaturization of biomedical studies (Nilsson *et al.* 2009).

One of the early single-particle studies in the pharmaceutical field was on the dissolution rate kinetics of individual compressed spherical tablets of benzoic acid (Parrott *et al.* 1955). While still rare, some single-particle and single-crystal studies have been published in recent years (Börjesson *et al.* 2013; Østergaard *et al.* 2011; Marabi *et al.* 2008; Prasad *et al.* 2002; Raghavan *et al.* 2002). By studying single particles, the cohesive interactions between particles can be ignored and the particle shape and size can be assessed. The single-particle approach thus minimizes the assumptions regarding factors influencing the dissolution rate. While, according to Aristotle: ”the whole is greater than the sum of its parts”, it can nevertheless be

argued that the whole is determined by its individual parts. This is also the case with powders and powder dissolution, where the primary particles composing the bulk are the main determinants of the overall bulk properties (de Villiers 1996). Single-particle analysis by image-based microscopy could therefore provide a promising novel approach to pharmaceutical material property characterization and thus demands further investigation.

3 Aims of the study

The aim of this thesis was to investigate the applicability of image-based microscopy of single-particles for physicochemical characterization of materials. In addition, a second aim was to develop a non-specific method and miniaturized devices capable of accurate, small-scale and rapid characterization and profiling of physicochemical properties of matter.

More specifically, the objectives of this dissertation were to:

- investigate and verify the applicability of image-based microscopy as an analytical technique for dissolution rate measurement from single-particles (**I**);
- develop a non-contact single-particle trapping device and extend the image-based analysis method to measure the IDR from individual freely rotating microscale particles (**III**);
- extend the image-based single-particle method for rapid miniaturized measurement of solubility (**II**);
- further miniaturize the single-particle method and device, in order to enable analysis of individual powder crystals, and to extend the method to lipophilicity and pK_a measurement (**IV**).

4 Experimental

4.1 Materials

4.1.1 Solutes

A total of 19 model compounds: acetylsalicylic acid (ASA) (Orion Pharma, Espoo, Finland), bioactive glass S53P4 (BonAlive Biomaterials Ltd, Turku, Finland), celecoxib (Kemprotec, Carnforth, UK), citric acid monohydrate (Mallinckrodt Baker B.V., Deventer, Holland), dicalciumphosphate 2-hydrate (Chemische Fabrik Budenheim KG, Budenheim, Germany), furosemide (Orion Pharma, Espoo, Finland/TCI Europe, Zwijndrecht, Belgium), hydrochlorothiazide (Alfa Aesar, Lancashire, UK), hydrocortisone (Fagron GmbH, Barsbüttel, Germany), ibuprofen (Orion Pharma, Espoo, Finland), indomethacin (Hawkins, MN, USA), human recombinant insulin (SAFC Pharma, MO, USA), itraconazole (Orion Pharma, Espoo, Finland), ketoprofen (Orion Pharma, Espoo, Finland), naproxen (Orion Pharma, Espoo, Finland/ICN Biomedicals Inc., OH, USA), paracetamol (PCM) (Oriola, Espoo, Finland/Hawkins, MN, USA), phenytoin (Orion Pharma, Espoo, Finland), probenecid (Sigma-Aldrich Chemie Gmbh, Steinheim, Germany), theophylline (TP) anhydrate (BASF, Ludwigshafen, Germany) and sodium chloride (Riedel-de Haën GmbH, Seelze, Germany) were used in the studies. The compounds were used without further purification and chosen to represent a maximum variability in solubility and chemical properties. The solubility range covered is above 9 log units, ranging from very soluble to practically insoluble.

4.1.2 Solvents

Distilled water, ultrapure deionized (MilliQ) water, ethanol (Altia, Rajamäki, Finland), octanol (YA Kemia, Helsinki, Finland), phosphate buffer solutions (*pH* 2.0, 3.0, 4.5, 5.8, 6.8, 8.0) and buffer solution (*pH* 9.0) prepared according to the European Pharmacopoeia 8.8 chapter 4.1.3. (Ph.Eur. 2015), phosphate-buffered saline (PBS) solution (Sigma-Aldrich, pH 7.4), as well as fed state simulated intestinal fluid (FeSSIF), fasted state simulated intestinal fluid (FaSSIF) and fasted state simulated gastric fluid (FaSSGF), prepared according to the manufacturers' instructions, were used as solvents.

4.2 Methods

4.2.1 Single-particle devices

4.2.1.1 Semi-static setup (setup 1) (I)

The semi-static dissolution of individual pellets was performed at ambient temperature (23 ± 0.5 °C) in 24-well plate wells containing 3 mL of degassed distilled water. In order to achieve a homogenous sample for UV spectrophotometric analysis, the well plate was shaken by turning three times, with a frequency of 1 turn/s, before sampling. This was performed approximately 30 s before sample collection, which allowed a suitable time-frame for the particle to settle at the bottom of the well, and for repositioning of the well plate, in order to allow simultaneous particle imaging. Between sampling-points the well plate was kept undisturbed.

Dissolution rate measurements of each substance were performed in triplicate, with dissolution times for the studied substances ranging between one and a few hours. Depending on the initial weight of the particle, sampling points were at 2, 5 and 10 min, and after this at intervals of 5 or 10 min. When approaching the end of a measurement in which 10 min intervals were used, the sampling rate was again shifted to every 5 min, increasing the frequency of data points. A measurement was continued until the particle size had decreased, so that a pellet no longer could be found when repositioning the well plate.

4.2.1.2 Hydrodynamic vortex particle trap (setup 2) (II-III)

Two issues had to be overcome in order to allow continuous imaging of particles under continuous flow conditions. First, the particle had to be positioned and remain in a confined area that would allow imaging using a stationary camera and a fixed magnification; second, the time consuming step of manual affixation by either gluing or clamping, which has generally been used to achieve particle positioning, was to be avoided (Østergaard *et al.* 2011; Marabi *et al.* 2008; Prasad *et al.* 2002; Raghavan *et al.* 2002). Apart from being time-consuming, particle fixing is likely to alter the surface morphology, intra-particle lattice energies and, thus, the dissolution kinetics of the particles. These challenges were met by design of a flow-through dissolution vessel incorporating a hydrodynamic particle trap (Fig. 2). The trapping mode of the dissolution cell was achieved by two tangential counter-flow solvent inlets. This resulted in a centrally positioned particle trapping vortex, allowing rapid non-contact particle focusing of the individual pellets and, consequently, continuous monitoring by optical microscopy.

Moreover, the rotational freedom of a particle in the vortex removes another common problem in particle size analysis, *i.e.* the settling of particles in a preferential orientation, denying the possibility of a 3D estimation of the particle size from one detection angle, an issue also present when studying fixed particles (Allen 1990). In this setup, where particles are allowed to rotate randomly within the particle trapping zone, an averaged 3D-shape and -size characterization is possible by the use of one image sensor and one detection angle only.

During a measurement at ambient temperature (22±1 °C), 20 mL of degassed distilled water, sufficient to maintain sink conditions for all substances during the dissolution process, was pumped by a peristaltic pump (Watson-Marlow 503U, Smith & Nephew, Falmouth,

Cornwall, England) in a closed loop with a constant flow rate of 10 ±0.05 mL/min through the dissolution cell. The solvent was kept in a closed vial under constant stirring. Still images of a dissolving freely rotating particle were acquired with a frame rate of 2-60 frames/minute, using stroboscopic illumination of the particle. All measurements were done in triplicate.

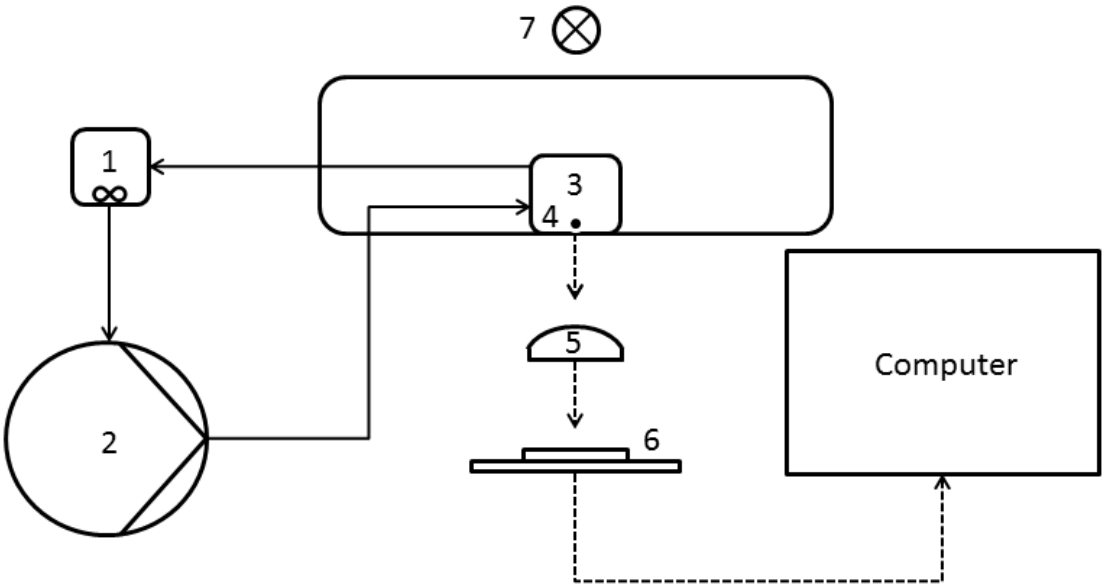

Figure 2. Schematic of the hydrodynamic vortex trap (not to scale). Degassed distilled water (**1**) (22±1 °C) was pumped (**2**) in a closed loop with a constant flow rate of 10 ± 0.05 mL/min through the dissolution cell (**3**), back to the vial (**1**). Still images of the dissolving rotating particle (**4**) were acquired through a magnifying lens (**5**) by a CMOS image sensor (**6**) with a frame rate of 2-60 frames/minute, using stroboscopic illumination (**7**) of the particle. Copyright © (2015) American Chemical Society, modified with permission from publication (**II**).

4.2.1.3 Membrane immobilization flow-through device (setup 3) (IV)

In order to allow the analysis of individual powder grains, a third flow-through device setup was developed (Fig. 3). The setup comprises a reaction chamber in which individual powder grains are immobilized on a membrane by the solvent flow across the particles and through the membrane. The flow-through device consisted of two resistant metal plates. The lower plate hosted a 1 mm outlet channel and the top plate hosted the inlet channel as well as a glass window to facilitate imaging. A 0.2 µm polycarbonate membrane filter (Whatman Nuclepore Track-Etched Membrane) was placed on the bottom plate and the particles to be analyzed were placed on top of this filter. The reaction chamber was tightly sealed before the start of a measurement.

During a measurement, solvents were degassed and pumped (Agilent 1260 Infinity Quaternary Pump) through the flow-chamber in an open configuration, with a constant flow rate of 1 mL/min. The temperature was adjusted by flowing the solvent through a thermostatted column compartment (Agilent 1200 Series). Imaging was performed through the transparent top part of the reaction chamber with a frame rate of 1-9 frames per second (fps). Data was collected from at least five individual grains, for all samples.

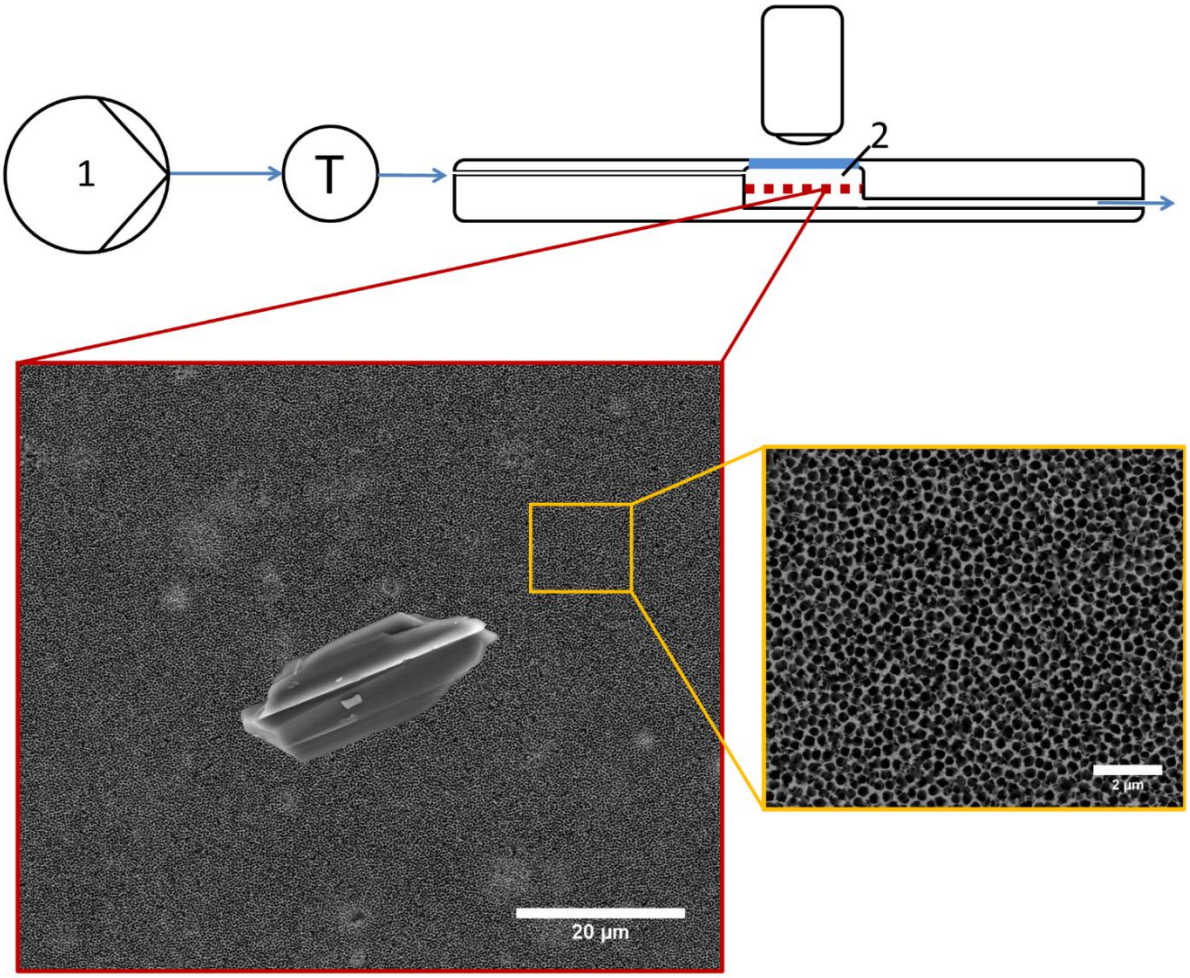

Figure 3. Schematic of the membrane immobilization flow-through device. The device consists of a pump (**1**), thermostatted column compartment (**T**) and a reaction chamber (**2**). The reaction chamber is horizontally divided into two by a membrane filter, on top of which the particles are immobilized. Imaging of the particles is enabled though the transparent cover glass. The first inset shows a SEM montage image of an individual itraconazole crystal on top of a membrane filter (to scale). The second inset shows a close-up SEM image of a membrane.

4.2.2 Micro-pellet production (I-III)

Bulk powders of the substances were pelletized using a custom built miniaturized extrusion-spheronizer. The substances were first ground for 5 minutes, which had been proven in preliminary studies to produce a primary particle size of approximately 10 µm. Depending on the wettability of a particular substance, an appropriate amount of distilled water was added to the micronized powder in order to produce a wetted mass for extrusion. Depending on the desired pellet size, the wetted mass was extruded through a perforated steel plate with an orifice diameter of 0.3-1 mm. The extrudates were then immediately spheronized into micro-pellets in the mini-spheronizer. Pellets were stored in a silica gel desiccator until being used in an experiment. All pellets were weighed using either an analytical balance (d=0.01 mg) (DeltaRange AX105, Mettler-Toledo GmbH, Greifensee, Switzerland) (**I**), or a mass comparator (d=1 µg) (AT21 Comparator, Mettler Toledo, Switzerland) (**II-III**).

4.2.3 UV-spectrophotometry (I)

Liquid samples were analyzed with a UV spectrophotometer (UV-1600PC Spectrophotometer, VWR International, Leuven, Belgium). The calibration curves were plotted from samples ranging over a ten-fold difference in concentration for ASA (200.0 nm, n = 6, R^2 = 0.997), PCM (243.9 nm, n = 8, R^2 = 1.000) and TP (203.2 nm, n = 10, R^2 = 0.999). Samples from three different time-points of one ASA, PCM and TP single-particle dissolution experiment were measured with and without filtrating. No systematic difference in detected absorbance was found between filtered and non-filtered samples, and the concentration difference was on average below 1%. Filtration was therefore determined as not being necessary in this case.

4.2.4 X-ray powder diffraction (I-III)

To confirm the solid-state transformation of TP anhydrate to TP monohydrate during the extrusion-spheronization process, intact and powdered pellets were analyzed with a theta-theta X-ray diffractometer (D8 advance, Bruker AXS GmbH, Germany). The measurements were performed in symmetrical reflection mode using Cu Kα radiation (λ=1.54 Å) over the angular range 2.5° to 20°, with a step size of 0.01° and a measuring time of 0.5 s/step. The analysis showed a conversion to monohydrate form throughout the pellets.

4.2.5 Imaging

Images were captured by USB-microscopes [DigiMicro 2.0 Scale, dnt Drahtlose Nachrichtentechnik Entwicklungs- und Vertriebs GmbH, Dietzen-bach, Germany (**I-III**)/Gigastone S1-100, Gigastone, CA, USA (**IV**)], using the accompanying software. In setup 1 and setup 2 the USB-microscope was used in inverted mode and particles were imaged through the transparent bottom of a well plate (**I**) or on-chip device (**II-III**). In setup 3 the USB-microscope was mounted on an upright Leica DMLB microscope with a Leica 50x (N Plan L50X/0.50 – ∞/0/C) objective (**IV**). The microscopes were calibrated with a micrometer graticule before each experiment.

Morphology of the powder grains and the membrane filter was assessed by scanning electron microscopy (SEM) (**IV**). The samples were adhered to a sample holder using double-sided carbon adhesive tape and Pt coated in a high vacuum evaporator (Q150TS, Quorum Technologies, UK). The samples were then imaged using a Quanta 250 FEG SEM (FEI Company, USA).

4.2.6 Image and data analysis

Images from setup 1 (**I**) were generally of good quality and easily segmented, without the need for any substantial removal of background noise. After binary conversion the images were analyzed using the built in particle size analysis tool of the public domain ImageJ software (ImageJ 1.46r, U.S. National Institutes of Health, Bethesda, Maryland, USA). In order to

compare the dissolution profiles acquired by UV spectrophotometry and image analysis the FDA advocated similarity factor f_2,

$$f_2 = 50 \times \left[\left(1 + \left(\frac{1}{n}\right) \sum_{t=1}^{n} (R_t - T_t)^2\right)^{-0.5} \times 100\right] \quad (22)$$

and difference factor f_1,

$$f_1 = \left[\frac{\left(\Sigma_{t=1}^{n} R_t - T_t\right)}{\left(\Sigma_{t=1}^{n} R_t\right)}\right] \times 100 \quad (23)$$

where n is the number of samples, R_t is the percental amount dissolved of the reference curve at time t and T_t is the percental amount dissolved of the test curve, at the same time-point, were applied (Costa & Sousa Lobo 2001; FDA 1997). UV-spectrophotometric profiles were used as reference in all the calculations. The f_2 equation gives the logarithmically converted sum-squared error of the two profiles, over all data points, and receives a value between 0 and 100 depending on the similarity. Two dissolution curves are regarded as similar for f_2 values over 50, which indicates an average of less than 10% difference (FDA 1997). The difference factor, on the other hand, gives the percentage difference between two curves over all data points, with a value below 15 considered as proving equivalency.

The similarity and difference factors can be calculated from data sets of more than four data points (FDA 1997). The values are, however, also susceptible to the number of sampling points, with a higher n value leading to better correlation. Therefore, it is suggested that no more than one sample, past the point where 85% of the initial mass has dissolved, should be used. In this study, however, it was important to compare the dissolution curves over the whole range from 0 to 100%. It was therefore decided that ten data points from the mass normalized dissolution curves would be enough to allow accurate assessment of the f_2 and f_1 values, and few enough not to cause an improvement of the data. Thus, the data points were calculated with 10% increments from fitted curves, so that the final time-point of an experiment was the 100% data point. 95% confidence intervals were additionally calculated for the collective data to visualize and compare the variance of the image and UV analysis data.

For the processing and analysis of images from setup 2 (**II-III**) a custom made MatLab –script was developed. Using this script, images are first enhanced by removing noise and improving contrast. Subsequently, the micrographs are converted into binary and a projection area equivalent sphere volume is calculated. Particle characteristics such as aspect ratio and perimeter are also acquired (**I-III**). For setup 3 (**IV**) a similar MatLab -script was developed. Using this script, a ROI containing an individual particle is first selected. The background is then removed from the ROI images and the micrographs converted into binary form, using local thresholding for each image. Furthermore, a particle is measured and the acquired data converted via equivalent circle and spheroid approximations into particle parameters.

In order to demonstrate the viability of random rotation 2D projection area averaging for 3D particle size and shape characterization, a MatLab –script was developed that randomly rotates selected 3D objects of known volume and surface-area (**III**). The script captures 1000 2D projection images in a sequence of every 100th random orientation. A projection surface area equivalent sphere approximation is subsequently performed and the acquired sphere surface-area and volume values compared with known values. The random rotation simulation data was also used to determine the required minimum number of images for reliable shape estimation, determined as the point where the moving average of the subsequent simulation

volume values decreased below 5% of the total average. The simulation was performed on several pharmaceutically relevant shapes, including equidimensional, elongated and flat morphologies with rounded and angular edges.

A real-time determination point was estimated in two ways. A 100 data-point moving average value was used in setup 2 (**II-III**). The early detection point was chosen as the moving average value, where the relative standard deviation (%RSD) of 100 moving average values decreased below the standard experimental error of 5. For experiments in which less than 200 data-points were acquired, the end-point of an experiment was considered as the determination time point. For setup 3, a two-sample (n=10) t-test analysis on the slope of the linear regression line of the decreasing particle radius was used. The slope was assumed to have reached steady state when the p value of the t-test analysis decreased below 0.05

5 Results and discussion

5.1 Single-particle dissolution rate (I)

5.1.1 Equivalent sphere volume approximation

As seen in Equations 14 and 20 the dissolution rate of a compound can be determined either from the cumulative increase in the solvent or from the cumulative mass released from the solid. Accordingly, the dissolution rate of an individual dissolving particle was calculated based on image analysis particle size decrease data. The initial mass of a pellet was acquired by weighing and the density of the pellets were assumed to be uniform throughout. This assumption was based on interpellet density data, which was found to be very similar, therefore, also the intraparticle density was assumed to be uniform. Moreover, it has been shown that the density of crystalline masses does not affect the dissolution rate, and that the density of pellets is primarily dependent on the density of the bulk material used in production (Löbmann *et al.* 2014; Sousa *et al.* 2002; Parrott *et al.* 1955). The use of pure substance pellets also meant that the relationship between decrease in particle size and mass released was directly proportional.

As the particles in setup 1 dissolved under stagnant conditions, and were imaged from only one angle, this meant that the analyzed particles were preferentially orientated at the moment of image capture (see section 2.4.1). However, since spheres show the same two-dimensional projection in all directions, the angle of observation is not relevant. The sphere is also the geometrical shape with the lowest surface area per volume ratio, and thus with the lowest surface energy. It is therefore expected that the spherical shape is the most geometrically stable and, accordingly, the shape which will dissolve most isotropically. This was found to be the case through the assessment of average aspect ratios of the particles. In line with results from other single-particle studies, the aspect ratio of a particle remained practically unchanged during the dissolution process, which indicates the retaining of a spheroidal shape throughout the experiments (Marabi *et al.* 2008; Parrott *et al.* 1955).

As was shown by Østergaard and coworkers, the concentration around a dissolving particle, in a stagnant liquid, is always highest towards the bottom of the dissolution vessel (Østergaard *et al.* 2011). This would cause varying concentration gradients and convection around the single pellets, which would lead to anisotropic dissolution. No significant increase in the aspect ratios during the single-pellet studies were, however, observed in this study. Isotropic dissolution could therefore be assumed, justifying the use of an equivalent sphere approximation when calculating particle volumes (Allen 1990).

5.1.2 Comparison of UV analysis and image analysis data

Data of the individual particles is presented in Table 2. It can be seen that the correlation data of the ASA and PCM pellets are very good, with average ±sd R^2 values of 0.988 ±0.013 and 0.989 ±0.01, and average f_2 values 76 ±27 and 80 ±13, respectively (Eqs 22 and 23). The f_2 and f_1 values are even better, around 90 and 2, respectively, for two out of three ASA and PCM single-particle experiments, demonstrating almost identical dissolution profiles between image analysis and UV-spectrophotometric data (Figure 4).

Table 2. Correlation of image and UV analysis data from the single-pellet experiments of acetylsalicylic acid (ASAX), theophylline monohydrate (TPX) and paracetamol (PCMX), as well particle characteristics. The similarity (f_2) and difference factors (f_1) indicate a very high correlation between image and UV analysis data

Experiment	R^2	f_2	f_1	Mass (mg)	Density (mg/mm^3)
ASA1	0.974	45	15	0.20	0.67
ASA2	0.993	89	2	0.41	0.64
ASA3	0.998	94	1	0.66	0.62
TP1	0.980	81	3	0.45	0.66
TP2	1.000	96	1	0.85	0.67
TP3	0.996	96	1	0.27	0.67
PCM1	0.997	91	2	0.33	0.75
PCM2	0.971	65	6	0.21	0.80
PCM3	0.998	83	3	0.51	0.79

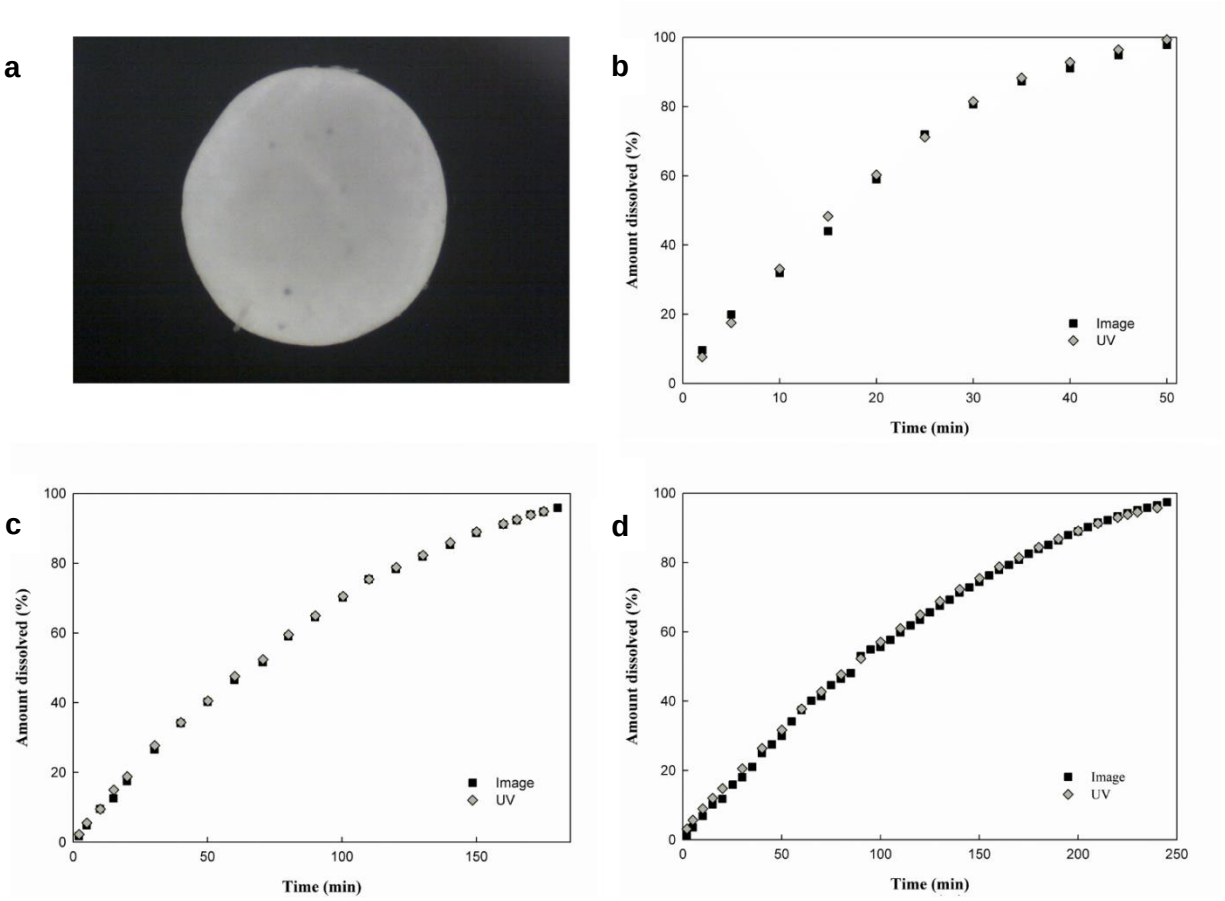

Figure 4. (**a**) A typical single-pellet image. Dissolution profiles of image and UV analysis data from paracetamol single pellet experiment (PCM1) (R^2=0.997) (**b**), theophylline monohydrate single pellet experiment (TP2) (R^2=1.000) (**c**), and acetylsalicylic acid single pellet experiment (ASA3) (R^2=0.998) (**d**). Copyright © (2014) Elsevier B.V., modified with permission from publication (**I**).

As the calibration curve for TP was produced using TP anhydrate, which is known to recrystallize as TP monohydrate after wetting, a correction factor of 1.0999, *i.e.* the *MW* ratio of TP anhydrate/TP monohydrate, was used to correct the UV absorbance data (Aaltonen *et al.* 2006). Using the correction factor data from all TP pellets showed very high similarity, with average f_2 and f_1 values of 91 ±9 and 2 ±1, respectively (Table 2).

The cause of the deviating variance of some of the profiles can be speculated upon. Image analysis data of PCM pellets had a narrower distribution, compared to UV-spectrophotometric data. This was a result of one deviating UV dissolution profile (PCM2) (Table 2). Accordingly, for ASA collective data, one deviating UV dissolution profile (ASA1) caused a slightly wider confidence interval for the chemical analysis data. The source for the weaker ASA1 and PCM2 correlations could be the pellet masses, which were the smallest of the three studied particles, consequently producing the most dilute samples. Chemical analysis of dilute samples is therefore assumed to be the main cause of error for these substances.

For TP monohydrate the case was reversed, with the image analysis data having a larger variance, due to the one deviating (TP1) dissolution profile. The data from experiment TP1 could have been predicted to be the most accurate of the three TP monohydrate pellets, since it had the lowest aspect ratio (1.09 ±0.07) and the highest roundness (0.92 ±0.05) throughout the experiment. However, the weight normalized TP1 dissolution curve from image analysis

data showed a slightly slower dissolution rate than absorbance data, and it is therefore assumed that the weighed mass of the TP1 pellet was the main cause of error.

In summary, the dissolution profiles acquired by traditional UV spectrophotometric analysis of liquid samples and image analysis of the dissolving pellets were practically identical. This result justifies the use of image-based microscopy as an analytical method for single-particle dissolution studies. The semi-static setup could be used, for example, to study the dissolution of inhalation particles or particles intended for buccal administration. As stated in chapter 2.4, optical microscopy could prove an optimal analytical tool for drug substances, as image analysis does not depend on the chemical properties of the analyzed substance. Due to this non-specific nature, image analysis could be used to study the whole domain of chemical space represented by NMEs and existing drugs. While image analysis has been used before in dissolution rate assessment, this is the first time, to the best of my knowledge, that it has been evaluated by comparison to existing analytical methods. The positive result enabled further extension of the single-particle methodology.

5.1.3 Single-particle intrinsic dissolution rate (SIDR) (III)

While IDRs are generally determined from the dissolution rate of a constant surface area, continuous monitoring and determination of a changing surface area of individual particles is an equivalent technique. Evidence of this was given already in single-particle studies conducted by Parrot and coworkers (Parrott *et al.* 1955). As sink conditions are required for facilitated determination, the flow through system of setup 2 was used in these studies. Additionally, in order to accurately determine the IDR, the effective surface area of the dissolving particle has to be known. An advantageous feature of setup 2 is that a random projection 3D particle morphology characterization can be made from the freely rotating pellet. It was observed in the random orientation simulation studies, that the particle surface-area was directly acquired from simulation projection area equivalent sphere surface area calculations, with an average deviation of 3.9%. This means that no extra shape factor needs to be considered when determining the SIDR effective surface area of a randomly rotating particle, thus, minimizing error sources.

In contrast to the sphere (**I**), the volume was not directly acquired from projection area equivalent sphere volume calculation for non-spherical rotating particles. Using random orientation circularity (c),

$$c = \frac{4\pi A}{p^2} \tag{24}$$

as a proxy for average particle sphericity, where A is the projection surface area and p is the projection area perimeter, the actual volume was determined to within on average 10.9% (Blott & Pye 2007; Cox 1927). Thus, it is possible to acquire both the particle surface area and volume throughout experiments in the vortex particle trap.

It can be noted that the volume data improved after circularity correction for all other particle shapes except the sphere. Theoretically a perfect sphere should produce a 1:1 equivalency of the equivalent sphere volume and true volume (**I**). The discrepancy with circularity correction can be explained by the effect of image analysis, as the pixelated perimeter will differ from the perfect sphere perimeter and will therefore distort the data, instead of correcting it. However, a drug particle will never be perfectly spherical and, thus, the

issue is purely theoretical. A practical weakness of characterizing 3D morphologies based on 2D projection images is that depressions and hollows in particle surfaces remain invisible. This is, however, an issue in most projection based characterization applications, but is considered to be less pronounced in dissolution studies, as dissolving particles strive towards surface energy minimization and, thus, increasing convexity during the dissolution process.

Highly reproducible SIDRs (Relative standard deviation [%RSD] = 9.4) were acquired for the eight studied substances, using the method established for volume and surface-area quantitation through the random orientation simulation. In line with previous research, the correlation between SIDR and literature equilibrium solubility values is excellent, with the exception of citric acid (Table 3 and Figure 5) ((**II**); Shah & Nelson 1975; Hamlin *et al.* 1965; Higuchi *et al.* 1965; Parrott *et al.* 1955).

Table 3. Substance, single-particle intrinsic dissolution rate (SIDR) and real-time data

Substance	Particle mass (µg)	Equilibrium solubility (mg/mL)[a]	SIDR (mg/cm^2/min)[a]	Average SIDR (mg/cm^2/min)[a]	Real-time SIDR (mg/cm^2/min)	% of dissolution profile needed
Naproxen	14	1.6×10^{-2}	1.9×10^{-3}	1.8×10^{-3}	1.9×10^{-3}	20.8
	31		1.7×10^{-3}			
	38		1.9×10^{-3}			
Furosemide	68	3.6×10^{-2}	4.3×10^{-3}	3.7×10^{-3}	3.7×10^{-3}	23.5
	121		3.7×10^{-3}			
	158		3.0×10^{-3}			
Hydrocortisone	47	3.2×10^{-1}	2.7×10^{-2}	2.8×10^{-2}	1.9×10^{-2}	20.0
	50		3.0×10^{-2}			
	60		2.6×10^{-2}			
Acetylsalicylic acid	36	4.6	4.8×10^{-1}	4.3×10^{-1}	3.7×10^{-1}	18.0
	43		4.1×10^{-1}			
	78		3.9×10^{-1}			
Theophylline	309	8.33	5.9×10^{-1}	6.2×10^{-1}	5.1×10^{-1}	32.8
	317		6.2×10^{-1}			
	25		6.5×10^{-1}			
Acetaminophen	202	14	1.2	1.2	1.1	31.7
	238		1.4			
	431		1.0			
Sodium chloride	548	317	38	36	N/A	N/A
	657		35			
	747		35			
Citric acid	156	592	40	36	N/A	N/A
	210		34			
	259		35			
Average						24.5

[a]In water at 20-25 °C, equilibrium solubility values from (US National Library of Medicine 2014; O'Neil 2001).

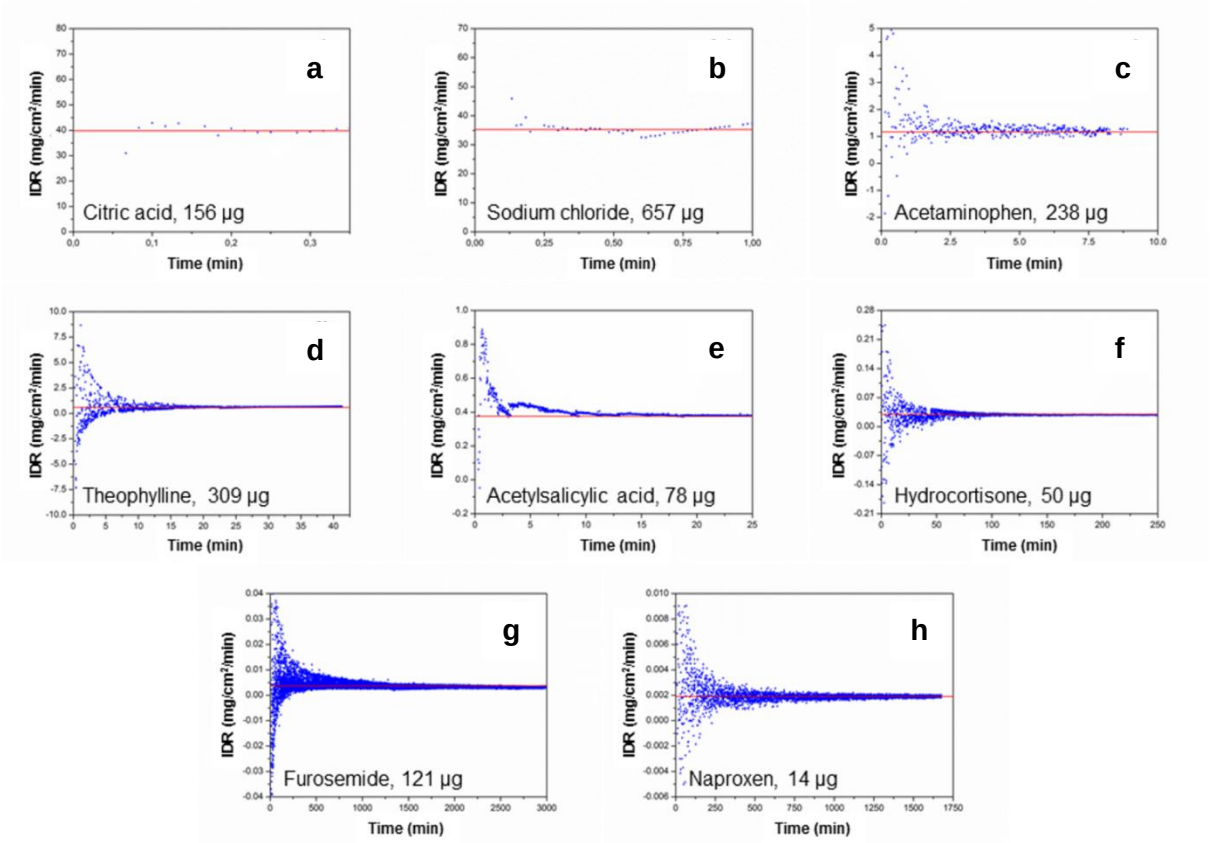

Figure 5. Single-particle intrinsic dissolution rate (SIDR) profiles of all studied substances. A progressive gravitation toward the average is observed, which allows earlier termination of the SIDR measurement for real-time high-throughput applications. The effect of intermittent rotation is depicted in the 78 µg acetylsalicylic acid SIDR profile (**e**). Copyright © (2015) American Chemical Society, modified with permission from publication (**III**).

In the random orientation simulation, an average of 33 ±13 random projection images were needed to move within a variance of 5% of the total average. This showed that a minimum of around 50 images would be required for accurate SIDR determination. Due to the very rapid dissolution rate of citric acid, the average number of images from these measurements was 22. Thus, it can be concluded that citric acid SIDR values are not as reliable as for the other substances. If citric acid is omitted from the comparison with literature equilibrium solubility values, a R^2 value of 0.999 is achieved for the linear fit intercepting origin (Figure 6a). As seen in Figure 5, the continuous rotation of the dissolving particles results in an evenly fluctuating profile around the average SIDR value. On the other hand, the effect of intermittent rotation on the SIDR profile, as seen with the 78 µg ASA particle (Figure 5e), leads to increased deviation from the average, and longer determination times.

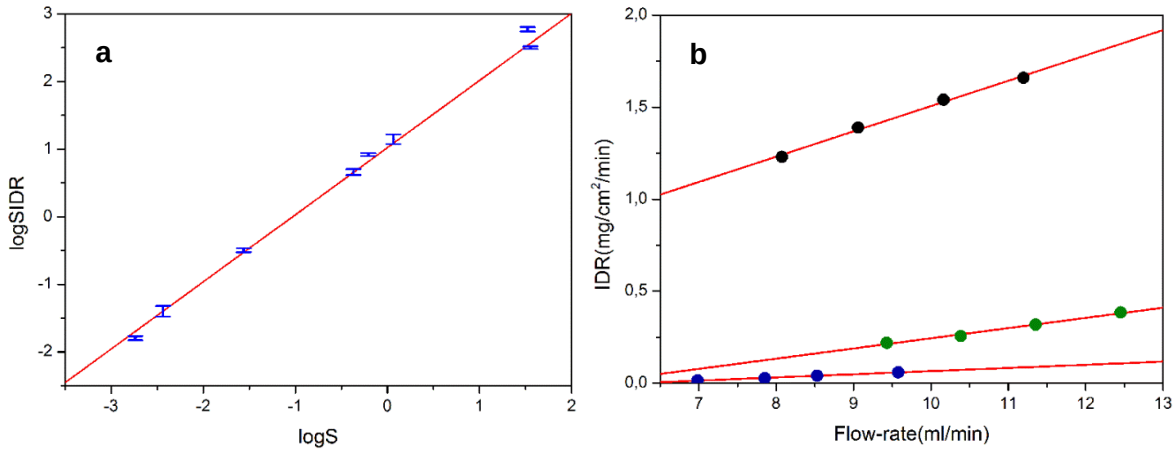

Figure 6. (**a**) Comparison of single-particle intrinsic dissolution rate (SIDR) and literature equilibrium solubility (log*S*) values. Logarithmic axes are used for clearer depiction. A high linear correlation (R^2=0.999) is observed, except for the citric acid data point in the upper right corner of the graph. (**b**) Relationship between flow-rate and SIDR in the optofluidic flow-through device. Paracetamol (●), R^2=0.995. Acetylsalicylic acid (●), R^2=0.989. Hydrocortisone (●), R^2=0.989. Copyright © (2015) American Chemical Society, modified with permission from publication (**III**).

The linear relationship between angular velocity of the rotating disc and measured DIDR of the compendial rotating disc Wood's apparatus is well reported (Tsuji *et al.* 1978; Shah & Nelson 1975; Levich 1962). Differing liquid flow dynamics have also been shown to produce variation in the IDRs for the same substances in different flow-through devices (Hulse *et al.* 2012; Lehto *et al.* 2008). Thus, the effect of flow rate was determined for setup 2, in order to allow comparison between the SIDR method and other flow-through apparatus, as well as the conventional DIDR apparatus. The characterization of the impact of flow-rate on SIDRs produced a linear relationship for the three studied substances, with R^2 values of 0.995, 0.989 and 0.989 for PCM, ASA and hydrocortisone, respectively (Figure 6b).

When high-throughput application is the goal, measurements should be automated and analysis performed in real-time (Kerns 2001). When using the %RSD of 5 as a threshold, an average of 24.5±12.1% of the total dissolution curve was needed for reliable SIDR determination (Table 3). This can be compared to conventional DIDR studies, where data from the first 10% of a dissolution curve is usually required for IDR determination (USP 2015). The result is the average of six substances as citric acid and sodium chloride where omitted from the analysis due to the intrinsic rapidity, between 21-68 seconds, of these measurements (Figure 5). The average difference between the real-time and the final SIDR value was 15.0% for the six substances, demonstrating the possibility of using the earlier determination point for more rapid analysis. When considering the final data point of the citric acid and sodium chloride SIDR measurements as the determination point, a mean measurement time of 2 hours was required for real-time SIDR determination of all substances, with a median of 8.6 minutes.

While kinetic solubility accuracy, *i.e.* within an uncertainty of 1.7 log units, of the SIDRs is achieved in an average of 6 minutes, this uncertainty is, as discussed in section 2.3.2.2, not adequate for informed decision-making (Stuart & Box 2005). However, the very small sample size of as little as 14 µg gives a clear advantage of the SIDR method when compared to other miniaturized IDR methods (Hulse *et al.* 2012; Avdeef 2008). Also, SIDR measurement produces particle size and shape dependent data, which allows the possible extrapolation of the acquired data into other particle shape(distributions), size(distributions) and effective surface areas. Furthermore, a general trend of increased data accuracy and acquisition rapidity

of SIDR data was observed, with decreasing initial particle size of the pellets. This indicated that further miniaturization could lead to a further decrease in measurement times.

5.2 Single-particle physicochemical profiling (II, IV)

5.2.1 Solubility (II, IV)

As reviewed in section 2.3.2.2, all methods for measuring the solubility of substances are based on multiparticle systems and determined in the presence of excess solid. However, according to the generally accepted diffusion layer dissolution rate model (Eq. 14), the difference between saturation concentration and bulk concentration is the rate limiting factor in a dissolution process (Noyes & Whitney 1897). In order to accurately determine the diffusion layer of a particle, the size and shape of the particle have to be reliably determined. One way of achieving this is through single-particle analysis, thus avoiding population based estimations and other error sources arising from *e.g.* aggregation and agglomeration of multiparticle systems (Hulse *et al.* 2012; de Villiers 1996). Under the sink conditions produced in the flow-through cell of setup 2, the concentration gradient in the diffusion layer, at the solid-liquid interface, goes from saturation concentration adjacent to the solid surface to zero outside the diffusion layer (Figure 7) (Higuchi 1967; Nernst 1904). Consequently, equilibrium solubility becomes the rate limiting factor of dissolution and can be determined.

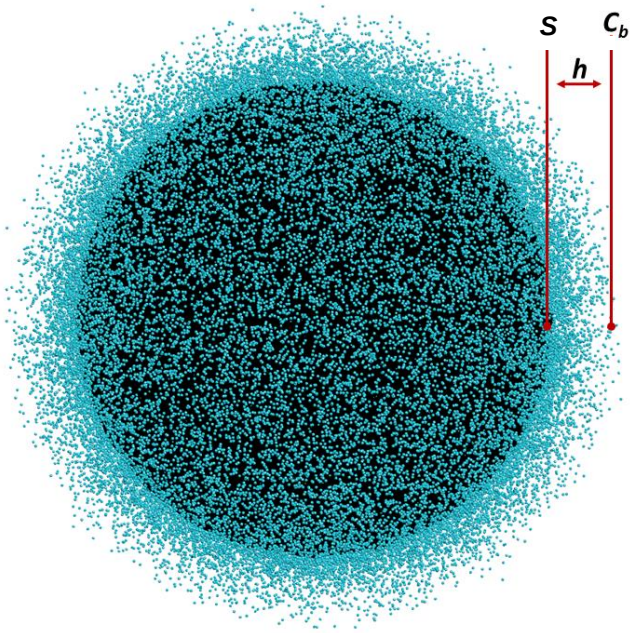

Figure 7. According to the diffusion layer model, equilibrium solubility S is assumed at the solid-liquid interface (black surface). A diffusion layer of thickness h (particles) exists immediately adjacent to the dissolving solid surface, outside of which a uniform bulk concentration C_b is assumed. The blue particles in the image represent dissolved molecules. Under sink conditions the bulk concentration is negligible and thus the equilibrium solubility at the solid-liquid interface becomes the rate limiting factor of dissolution, and can be determined. Copyright © (2015) American Chemical Society, modified with permission from publication (**II**).

By rearranging the Hixson-Crowell cube root equation (Eq. 18), an expression for solubility, based on single-particle dissolution, can be found. Using the expression for the dissolution rate constant K in Equation 19 (Wang & Flanagan 1999), the estimation of the diffusion coefficient D_c from Equation 16 (Al-janabi 1990), and approximating the diffusion layer thickness to 30 μm (Hintz & Johnson 1989), the rearranged equation gives,

$$S = \frac{\rho\left(w_0^{1/3} - {w_t}^{1/3}\right) MW^{1/3}}{\left(\frac{4\pi\rho}{3}\right)^{1/3} t} \tag{25}$$

As can be appreciated from the above equation, the only primary data needed for determining the solubility of a substance, from the dissolution rate, is the initial weight of the dissolving particle and the molecular weight of the dissolving substance. In accordance with image-based determination of single-particle dissolution rate (**I**), the pellet density is acquired from the initial mass of the pellet divided by the projection area equivalent volume (**II**). For crystals, the mass was calculated based on molecular weight of a compound and true density of the crystal, using a spheroid approximation for the crystal volume (**IV**). The crystal density for all organic and inorganic compounds were acquired from literature, whereas the crystal density of recombinant human insulin was acquired as the inverse of the partial specific volume of the protein monomer (Massera & Hupa 2014; Gbureck *et al.* 2007; Murphy *et al.* 1998; Allen 1990).

As was reviewed in section 2.3.2.2 the determination of solubility based on bulk solvent concentrations, requires several hours or even days to reach an equilibrated state between the solid and the dissolved molecules (Alsenz & Kansy 2007; Sugano *et al.* 2007; Lipinski *et al.* 1997). Contrarily, the buildup of the diffusion layer, for diffusivities common to drugs, has been shown to take approximately 0.02-2 s (Weiss 1996). One has to bear in mind that the solubility thus determined will be dependent on the solid form of the dissolving substance. For the most stable polymorph of a pure drug substance, the solubility determined will be the equilibrium solubility of the substance. If an unstable, a metastable form, salt, solvate or cocrystal is analyzed, the resulting solubility value will be the apparent solubility of that particular solid form. Therefore, in order to achieve values comparable to literature values, the substances chosen for this study were known not to undergo solid state transformations during the time range and in the environment of the dissolution process.

However, going forward it might be advantageous for drug development settings to study the apparent solubility of metastable forms. In salt and solid form screening, one aim is to improve the bioavailability of a substance by increasing the dissolution rate and apparent solubility (Sugano *et al.* 2007; Huang & Tong 2004). It may therefore be more valuable to study the apparent solubility of substances and to assess the stability of metastable forms during physiologically relevant conditions and timescales, such as the MITT of 1-3 h (Bhattachar *et al.* 2006; Dressman *et al.* 1998).

It is also well known that the diffusion layer thickness of a dissolving solid is affected by the hydrodynamic environment of the dissolution system (Levich 1962). Therefore, the data obtained from a specific dissolution system will be dependent on the specific conditions of that system, such as flow-rate of the solvent, which are reflected in a system constant. The system constant (k_s = 7.95 x 10^3) for setup 2 was acquired from the log-log linear correlation (R^2=0.998) between single-particle equilibrium solubility values and equilibrium solubility data from literature. By inserting this value into Equation 25,

$$S = 7.95 \times 10^3 \frac{\rho\left(w_0^{1/3} - {w_t}^{1/3}\right) MW^{1/3}}{\left(\frac{4\pi\rho}{3}\right)^{1/3} t} \quad (26)$$

it was possible to convert the measured single-particle solubility values into equilibrium solubility, achieving an average difference of 7.8% when compared to literature values and a RMSE of 0.07 log units for the single-particle solubility values (Table 4). The solubility values acquired in this way under unbuffered conditions, are the native equilibrium solubilities of the substances. A typical single-particle solubility profile obtained by Equation 26 is shown in Figure 8. It can be seen that a fluctuation around the equilibrium value takes place during the dissolution process, with the initially wide fluctuation equilibrating after a period of time.

Table 4. Comparison of single-particle and literature equilibrium solubility values

Substance	Single-particle equilibrium solubility (mg/mL) ± sd	Literature equilibrium solubility (mg/mL)	Difference from average %
Paracetamol	12.9 ± 2.2	14.0	- 8.0
Acetylsalicylic acid	4.57 ± 0.28	4.60	- 0.7
Citric acid monohydrate	626 ± 50	592	+ 5.7
Furosemide	0.033 ± 0.011	0.040	- 7.4
Hydrocortisone	0.29 ± 0.02	0.32	- 6.3
Naproxen	0.019 ± 0.003	0.016	+ 20.1
Sodium chloride	383 ± 10	317	+ 6.8
Theophylline monohydrate	7.75 ± 0.23	8.33	- 6.9
Average (absolute)			7.8

While more data is retrieved from more poorly soluble substances, an increased variability with decreasing solubility was observed, due to the longer dissolution times. A simple explanation is the relative increase in measurement error when studying small-scale changes. In a parallel experiment it was not possible to retrieve a dissolution curve for the low solubility single-particles using UV-spectrophotometric analysis. This was probably due to the adsorption and/or absorption of the low quantities of the hydrophobic substances to the tubing of the flow-through system, and shows the critical importance of minimizing error sources when using miniaturized methods. The use of image-based analysis is one way to achieve this, through the avoidance of potential error sources such as liquid sample handling and the influence of adsorption or absorption of substances to hydrophobic surfaces of the apparatus and equipment (Paakkunainen *et al.* 2009; Faller & Ertl 2007).

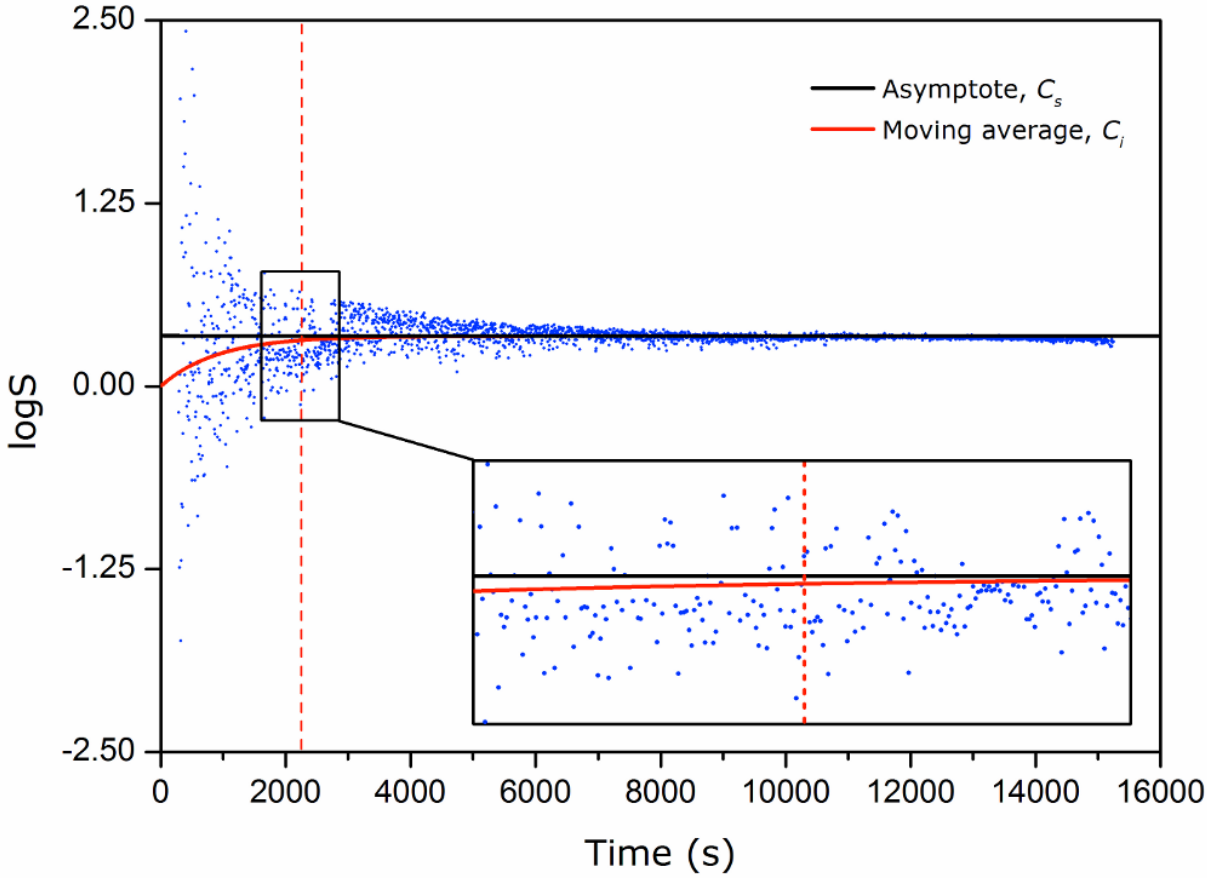

Figure 8. Single-particle solubility profile. The dots show individual single-particle solubility values acquired through the reorganized Hixson-Crowell cube root equation (Eq. 26). Data-points up to 290 seconds, with a higher range of fluctuation, are omitted in order to produce a more focused view. The moving average (n=100) represents the real-time characterization. In the inset, a close-up of the equilibration is visualized with the dashed vertical line indicating the real-time determination point. At this time-point, the equilibrium solubility value is on average within 8% of the final value for all substances. Copyright © (2015) American Chemical Society, reprinted with permission from publication (**II**).

In the trapping efficiency characterization of setup 2, a linear relationship between particle size and average deviation of the center of mass was observed for non-dissolvable particles (**III**). The focusing efficiency of the device is, thus, particle size dependent, with smaller particles being more effectively positioned. This is an advantage, as higher magnifications with narrower fields of view can be used for more accurate data acquisition, when studying smaller particles. However, particles below 100 µm tend to exit the device with the flow, thus posing a lower limit on the single-particle method of setup 2. The two other main limiting factors of setup 2 are the initial micro-pellet production and the initial mass determination of the individual particle.

5.2.2 Solubility, lipophilicity and charge state (IV)

In order to address the issues of setup 2 and to evaluate the possibility of more rapid analysis with decreasing particle size (**III**), setup 3 was developed. As described in section 4.2.1.3, individual particle grains are immobilized by the liquid flow toward a filter membrane, where they can be imaged. Similarly to setup 2, dissolved molecules are continuously extracted from the reaction chamber and the concentration profile around the individual particles is kept constant under sink conditions. Again, using Equation 25 the system constant for setup 3 was determined by correlating image analysis equilibrium solubility data with literature equilibrium solubility data (n=60, R^2=0.963), using 11 organic compounds of known water solubility, spanning over 7.5 orders of magnitude at the same temperature (Fig. 9).

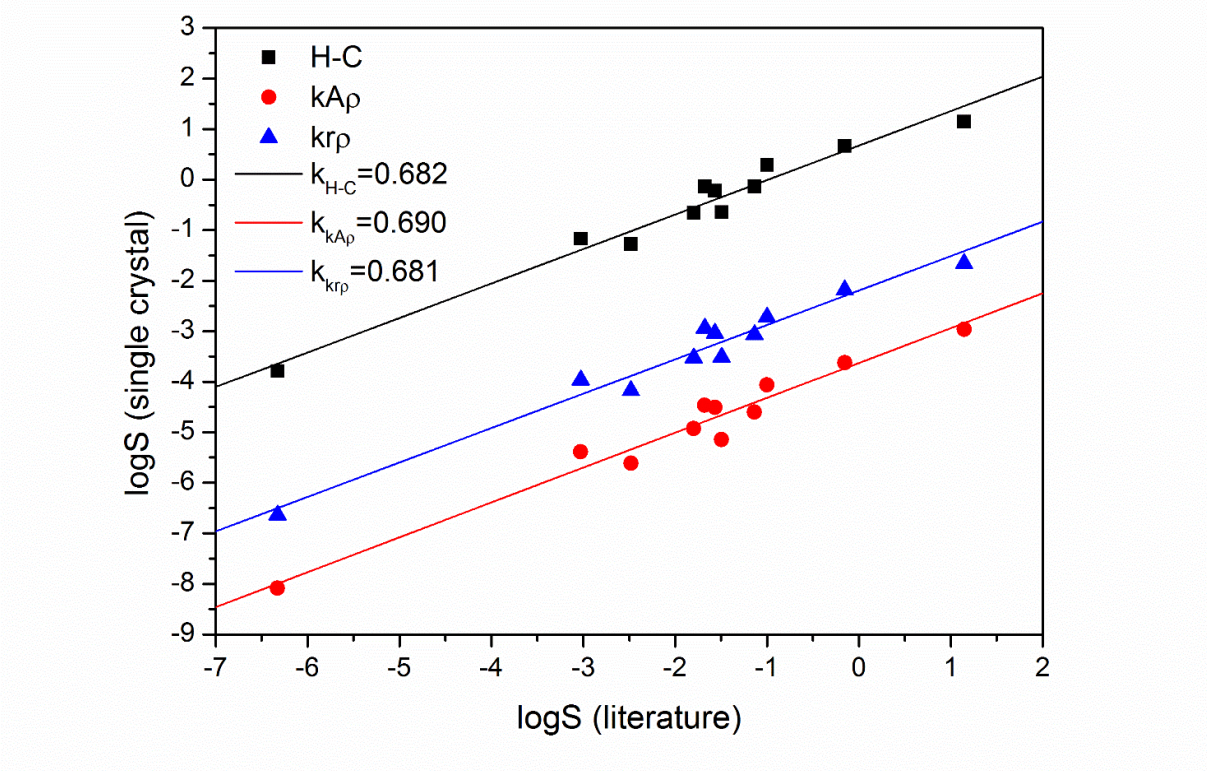

Figure 9. Calibration curves determined based on the diffusion layer dissolution rate equation (H-C), the density corrected slope of the decreasing projection area (kAρ) and the density corrected slope of the decreasing projection area equivalent circle radius (krρ). It can be seen that the slope of the calibration curves using different readout parameters do not differ substantially, with the density corrected radius and the dissolution rate equation calibration slopes being practically identical.

Additionally, it was found that the decreasing projection area slope, as well as the slope of the decreasing particle radius, gave almost similar correlation as the solubility calculated based on the dissolution rate equation (Fig. 9). The projection area was directly acquired from pixel data and the radius was calculated based on equivalent circle approximation. A slight improvement in the correlation was observed when multiplying the slope values with the respective crystal density of the studied material. Crystal density is an obvious affecting factor, as it directly relates to the mass released from the respective particle volume decrease. However, the difference between density corrected and non-density corrected data was on average 0.27 log units and thus within the range of uncertainty of the calibration data. This

implies that a reasonable estimation of the solubility can be acquired for a substance, even in cases where material properties are not known *a priori*, based on solely particle size data. The power of experimental measurement is highlighted by the fact that for two of the model compounds, indomethacin and probenecid, only 4% and 2%, respectively, of specifically trained computer models succeeded in accurately predicting the solubility (Hopfinger *et al.* 2009).

In order to demonstrate the non-specific and wide applicability of the method, the solubility in PBS solution was determined for additionally three model compounds of diverse chemical structure and properties; recombinant human insulin, dicalcium phosphate dihydrate ($CaHPO_4 \cdot 2H_2O$, DCPD, brushite) and bioactive glass S53P4. The difference between the single-particle values and literature values for all substances was on average 0.3 log units and the uncertainty of the single crystal solubility values 0.15±0.06 log units, which is substantially less than the range of uncertainty of current high-throughput and *in silico* methods (Tetko *et al.* 2009; Mannhold *et al.* 2009; Stuart & Box 2005; Jorgensen & Duffy 2002).

As the solid form of a compound has not necessarily been chosen at the discovery stage, and variation in crystal forms are common, an uncertainty of 0.3 log units, *i.e.* a twofold error, can be considered the highest achievable accuracy for crystalline material in drug discovery settings (Sugano *et al.* 2007; Kerns 2001). This is because the difference in solubility between different polymorphs and hydrate/anhydrate forms of the same drug substance has been found to generally differ twofold or less, while the difference in solubility between amorphous and crystalline material is more diverse and can show up to hundredfold differences (Pudipeddi & Serajuddin 2005; Huang & Tong 2004). Amorphousness and crystallinity can, however, be assessed by polarized light microscopy and the apparent solubility between the two can therefore be easily differentiated (Wu *et al.* 2014; Sugano *et al.* 2006).

In order to demonstrate HCA applicability of setup 3, the native, intrinsic and equilibrium solubility, dissolution rate, pK_a, *logP* and *logD* were determined for model substance indomethacin (Fig. 10). Indomethacin is a weakly acidic organic drug molecule, commonly used as a model compound for poorly soluble drugs. The *pH*-solubility profile was measured in aqueous buffers over the physiologically relevant range of *pH* 2 to 9. Additionally, the equilibrium solubility was determined in three simulated body fluids (fasted state simulated intestinal fluid, *pH* 6.5; fed state simulated intestinal fluid, *pH* 5; fasted state simulated gastric fluid, *pH* 1.6) as well as two commonly used organic solvents (ethanol and octanol) (Table 5). It can be observed from Figure 10, that the solubility increases linearly with the increasing ratio $[A^-]/[HA]$ of the acidic moiety, according to Equation 8. This is however not always the case and the application of the Henderson-Hasselbalch relation, in order to calculate solubilities, based on the intrinsic solubility, has been found to be limited, stressing the need for experimental determination (Bergström *et al.* 2004). The pK_a of 4.4 for indomethacin was acquired from the intersection of the mean intrinsic solubility value (S_o, *pH* 2-3) and the regression line of the linearly increasing *pH*-solubility profile. As the aqueous solubility of the unionized form as well as the solubility in octanol were acquired, it was possible to determine the *logP* value of indomethacin as 4.1, using Equation 11. Finally, from *logP*, pK_a and *pH* data, the *logD* profile was determined using Equation 12. The parameters are in high correlation with theory and literature data (Fig. 10, Table 6).

Thus, by only observing and characterizing one variable, *i.e.* the particle size decrease of an individual crystal, it is possible to mine, in a HCA manner, seven fundamental materials characteristics for a substance. The indomethacin profile was acquired from the analysis of less than 400 ng of compound in total (n=69). Using HCA of individual crystals, the total amount

analyzed for a full solubility-lipophilicity-charge state profile is thus above one order of magnitude less than the amount required for one experiment in one solvent using existing state of the art techniques (section 2.3.2.2).

Table 5. Indomethacin solubility profile

Solvent	*pH*	Clog$S_{particle}$[a] (g/L)	Equilibrium solubility, S[b] (g/L)	RSD (%)
Aq. Buff.	9.0	1.16×10^{0} (n=6)	1.45×10^{1}	55.2
Aq. Buff.	8.0	-1.97×10^{-2} (n=7)	9.56×10^{-1}	16.5
Aq. Buff.	7.4	-6.60×10^{-1} (n=5)	2.19×10^{-1}	48.9
Aq. Buff.	6.8	-1.24×10^{0} (n=5)	5.73×10^{-2}	50.1
Aq. Buff.	5.8	-1.86×10^{0} (n=5)	1.39×10^{-2}	35.0
Aq. Buff.	4.5	-3.13×10^{0} (n=5)	7.50×10^{-4}	31.5
Aq. Buff.	3.0	-3.46×10^{0} (n=5)	3.48×10^{-4}	10.1
Aq. Buff.	2.0	-3.54×10^{0} (n=5)	2.89×10^{-4}	18.8
FaSSIF	6.5	-1.84×10^{0} (n=6)	1.46×10^{-2}	34.2
FeSSIF	5.0	-2.32×10^{0} (n=5)	4.78×10^{-3}	26.7
FaSSGF	1.6	-3.51×10^{0} (n=5)	3.08×10^{-4}	19.3
Ethanol	n/a	1.16×10^{0} (n=5)	1.46×10^{1}	14.4
Octanol	n/a	6.37×10^{-1} (n=5)	4.34×10^{0}	8.22
Average				28.4

[a]Calculated values based on dissolution rate equation calibration data, [b]$10^{(ClogS_{particle})}$. Calculated log$S$ ($ClogS_{particle}$).

Table 6. Indomethacin lipophilicity/charge state profile

Parameter	Single-crystal	Literature ref.
pK_a	4.4	4.5[a]
logP	4.14	4.27[b]
$logD_{7.4}$	1.2	1.3[c]

[a](Hansch *et al.* 1995), [b](O'Neil 2001), [c](Barton *et al.* 1997).

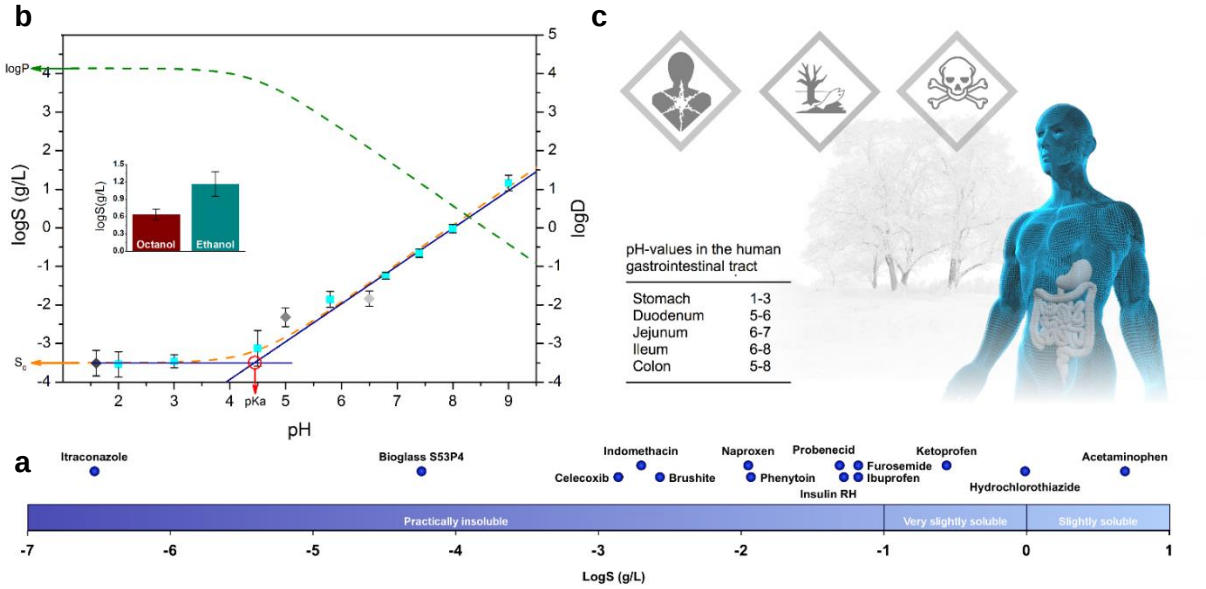

Figure 10. Solubility-lipophilicity-charge state profiling and impact. **(a)** The equilibrium solubilities (*S*) measured for a diverse set of organic, inorganic, and biological materials over a solubility range of 7.5 orders of magnitude. The Log*S* axis includes commonly used qualitative solubility ranges. **(b)** A complete solubility-lipophilicity-charge state profile for model compound indomethacin. Analyzing less than 400 ng of compound in total (n=69), the intrinsic (S_0) and equilibrium solubility, dissolution rate, pK_a, *logP* and *logD* (– –) were acquired; using organic solvents, aqueous (■), as well as simulated physiological solutions (◆◆◆). The parameters are in high correlation with theory (– –) and literature values (Table 6). **(c)** As solubility and lipophilicity determine the physiological and environmental activity and distribution of materials, HCA can be applied in determining for example local or systemic absorption, toxicity and therapeutic effects, as well as the environmental impact of compounds. Automated image-based analysis further enables rapid screening, with minimal compound consumption and handling of valuable and potentially hazardous compounds.

Using statistical real-time verification (t-test, $p \leq 0.05$), it was possible to terminate the individual measurements early on with a sufficient degree of accuracy. At the real-time determination point, the particle radius decrease slope differed on average 0.21 log units from the regression line slope of a full experiment. The uncertainty within the range of the RSD of the complete measurements and, again, substantially less than the uncertainty of standard methods (Tetko *et al.* 2009; Mannhold *et al.* 2009; Stuart & Box 2005; Jorgensen & Duffy 2002). With an image acquisition rate of 1 fps, the steady slope was reached generally within 30 seconds or after around 25 data points, regardless of the studied substance. Therefore, rather than being material dependent, the measurement time seems to be controlled by data acquisition speed and, thus, by the frame rate and resolution of the imaging sensor. For the least soluble compound studied, itraconazole, steady state was reached in 11 seconds with an image acquisition rate of 9 fps (Fig. 11).

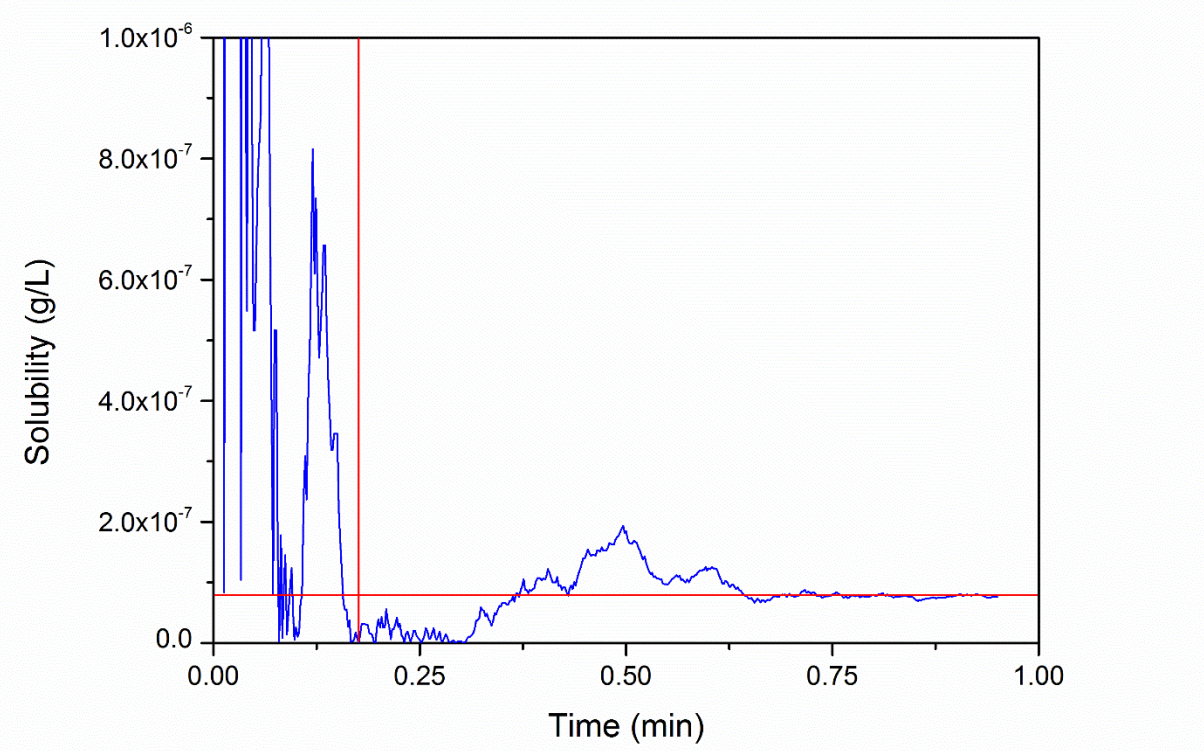

Figure 11. Itraconazole solubility profile. Calculated based on the decreasing slope of the individual particle radius. With an image acquisition rate of 9 fps the steady state (t-test, $p \leq 0.05$) real-time termination point was achieved after 0.18 min (n=96).

The average initial mass of the individual crystals analyzed was 5.0 ng. The substance needed for individual measurements using image-based HCA is thus above three orders of magnitude less than what is required in current state of the art miniaturized methods (section 2.3.2.2). The gain is much higher when comparing to standard methods, which operate in the mg and g range (OECD 2016a; OECD 2016b). Substantial advancements of the method capabilities can also be foreseen, as techniques for the determination of particle size and mass on the nanometer and femtogram scale already exist (Hell 2007; Greenbaum *et al.* 2012; Burg *et al.* 2007). Moreover, the smallest change in mass between two samples of ten after reaching steady state was 116 fg. This sets the limit of quantitation of image-based analysis on the same level as that of current advanced analytical methods, such as MS (Ternes 2001).

6 Conclusions

In this thesis the applicability of image-based microscopy of single-particles was explored as a novel method for physicochemical characterization of drugs.

First, it was shown that data obtained by optical image-based digital microscopy and UV spectrophotometry produce practically identical dissolution rate data with equal variance for dissolving individual particles of model acidic and basic drug compounds. Consequently, it is proposed that image analysis can be used, on its own, as a viable analytical technique in single-particle dissolution studies

Next, a single-particle trapping device was developed, wherein individual drug particles can be continuously imaged under constant flow conditions. Using this device it was shown that optical monitoring combined with image analysis can be used for rapid real-time determination of IDR from continuously changing effective surface areas of dissolving individual microparticles.

The method was then further extended to determine the equilibrium solubility of drugs. While solubility is generally determined from bulk solutions after long incubation times, it was shown that the equilibrium solubility can be rapidly determined from individual pure-substance particles based on the diffusion layer theory and image analysis.

Finally, a second device was developed and the method further miniaturized and extended to acquire seven fundamental physicochemical properties of matter, *i.e.* the native, intrinsic and equilibrium solubilities, dissolution rate, pK_a, *logP* and *logD,* with femtogram range accuracy, from individual nanogram crystals. Using the method, it is possible to acquire a complete pH-solubility profile for an unknown material of unknown composition in aqueous buffers, in addition to the solubility and dissolution rate in any transparent organic, aqueous or physiological solvent, with individual measurements of less than 30 seconds.

In summary, these results strongly suggest that image-based analysis of materials could be applied in HTE applications, as speed can be increased and substance consumption reduced, while maintaining analytical integrity. As in the case of kinetic solubility assessment, the non-specific nature of image-based analysis makes the method applicable to the whole range of chemical space of drugs, in various organic, aqueous and physiological solvents. In line with state of the art miniaturized methods such as CE, the nanogram range substance consumption and sub-minute range automated analysis makes the single-particle method applicable at the very beginning of the drug discovery process. Furthermore, the high accuracy as well as low detection limit and data variability, comparable to those of current 'gold standard' measurements and advanced analytical methods, indicates that image-based analysis could bridge the gap currently separating throughput and quality in physicochemical analysis. With automation and parallelization of the single-particle measurements, all the required criteria for HTE methods would be achieved.

Finally, the possibility of acquiring solubility, dissolution rate, lipophilicity and pK_a using a single analytical method could significantly simplify and speed up accurate data acquisition, leading to faster and more informed decision-making and, ultimately, better and more affordable drugs.

References

Aaltonen, J., Heinänen, P., Peltonen, L., Kortejärvi, H., Tanninen, V.P., Christiansen, L., Hirvonen, J., Yliruusi, J., Rantanen, J., 2006. In situ measurement of solvent-mediated phase transformations during dissolution testing. J. Pharm. Sci. 95, 2730–2737.

Al-janabi, I.I., 1990. An Approach for the Prediction of the Intrinsic Dissolution Rates of Drugs under Unbuffed Conditions. Drug Dev. Ind. Pharm. 16, 347–360.

Allen, F.H., 2002. The Cambridge Structural Database: a quarter of a million crystal structures and rising. Acta Crystallogr. Sect. B Struct. Sci. 58, 380–388.

Allen, T., 1990. Powder Sampling And Particle Size Determination 4th ed., Padstow: T.J. Press.

Almeida-Prieto, S., Blanco-Méndez, J., Otero-Espinar, F.J., 2006. Microscopic image analysis techniques for the morphological characterization of pharmaceutical particles: Influence of process variables. J. Pharm. Sci. 95, 348–57.

Alsenz, J., Kansy, M., 2007. High throughput solubility measurement in drug discovery and development. Adv. Drug Deliv. Rev. 59, 546–67.

Amidon, G.L., Lennernas, H., Shah, V.P., Crison, J.R., 1995. A theoretical basis for a biopharmaceutic drug classification: The correlation of in vitro drug product dissolution and in vivo bioavailability. Pharm. Res. 12, 413–420.

Avdeef, A., 2008. Miniaturized Rotating Disk Intrinsic Dissolution Rate Measurement: Effects of Buffer Capacity in Comparisons to Traditional Wood's Apparatus. Pharm. Res. 25, 2613–2627.

Avdeef, A., 2001. Physicochemical Profiling (Solubility, Permeability and Charge State). Curr. Top. Med. Chem. 1, 277–351.

Avdeef, A., 1998. pH- metric Solubility. 1. Solubility- pH Profiles from Bjerrum Plots. Gibbs Buffer and pKa in the Solid State. Pharm. Pharmacol. Commun. 4, 165–178.

Avdeef, A., Berger, C.M., 2001. pH-metric solubility. 3. Dissolution titration template method for solubility determination. Eur. J. Pharm. Sci. 14, 281–291.

Avdeef, A., Berger, C.M., Brownell, C., 2000. pH-metric solubility. 2: correlation between the acid-base titration and the saturation shake-flask solubility-pH methods. Pharm. Res. 17, 85–9.

Avdeef, A., Tsinman, K., Tsinman, O., Sun, N., Voloboy, D., 2009. Miniaturization of powder dissolution measurement and estimation of particle size. Chem. Biodivers. 6, 1796–811.

Bakal, C., Aach, J., Church, G., Perrimon, N., 2007. Quantitative morphological signatures define local signaling networks regulating cell morphology. Science 316, 1753–6.

Balogh, G.T., Tarcsay, A., Keserű, G.M., 2012. Comparative evaluation of pK(a) prediction tools on a drug discovery dataset. J. Pharm. Biomed. Anal. 67-68, 63–70.

Bangkedphol, S., Keenan, H.E., Davidson, C., Sakultantimetha, A., Songsasen, A., 2009. The partition behavior of tributyltin and prediction of environmental fate, persistence and toxicity in aquatic environments. Chemosphere 77, 1326–32.

Barton, P., Davis, A.M., McCarthy, D.J., Webborn, P.J., 1997. Drug-phospholipid interactions. 2. Predicting the sites of drug distribution using n-octanol/water and membrane/water distribution coefficients. J. Pharm. Sci. 86, 1034–9.

Bergström, C.A.S., Luthman, K., Artursson, P., 2004. Accuracy of calculated pH-dependent aqueous drug solubility. Eur. J. Pharm. Sci. 22, 387–98.

Bevan, C.D., Lloyd, R.S., 2000. A High-Throughput Screening Method for the Determination of Aqueous Drug Solubility Using Laser Nephelometry in Microtiter Plates. Anal. Chem. 72, 1781–1787.

Bhattachar, S.N., Deschenes, L.A., Wesley, J.A., 2006. Solubility: it's not just for physical chemists. Drug Discov. Today 11, 1012–8.

Blott, S.J., Pye, K., 2007. Particle shape: a review and new methods of characterization and classification. Sedimentology 55, 31–63.

Börjesson, E., Innings, F., Trägårdh, C., Bergenståhl, B., Paulsson, M., 2013. The dissolution behavior of individual powder particles. Dairy Sci. Technol. 93, 357–371.

Box, K., Bevan, C., Comer, J., Hill, A., Allen, R., Reynolds, D., 2003. High-Throughput Measurement of p K a Values in a Mixed-Buffer Linear pH Gradient System. Anal. Chem. 75, 883–892.

Bruner, L., Tolloczko, S., 1901. Über die Auflösungsgeschwindigkeit fester Körper. Zeitschrift für Anorg. Chemie 28, 314–330.
Burg, T.P., Godin, M., Knudsen, S.M., Shen, W., Carlson, G., Foster, J.S., Babcock, K., Manalis, S.R., 2007. Weighing of biomolecules, single cells and single nanoparticles in fluid. Nature 446, 1066–9.
Burggraeve, A., Sandler, N., Heinämäki, J., Räikkönen, H., Remon, J.P., Vervaet, C., De Beer, T., Yliruusi, J., 2011. Real-time image-based investigation of spheronization and drying phenomena using different pellet formulations. Eur. J. Pharm. Sci. 44, 635–42.
Cabot, J.M., Fuguet, E., Rosés, M., Smejkal, P., Breadmore, M.C., 2015. Novel Instrument for Automated pK(a) Determination by Internal Standard Capillary Electrophoresis. Anal. Chem. 87, 6165–72.
Comer, J., 2003. High-Throughput Measurement of Drug pKa Values for ADME Screening. J. Assoc. Lab. Autom. 8, 55–59.
Congreve, M., Carr, R., Murray, C., Jhoti, H., 2003. A “rule of three” for fragment-based lead discovery? Drug Discov. Today 8, 876–7.
Cook, D., Brown, D., Alexander, R., March, R., Morgan, P., Satterthwaite, G., Pangalos, M.N., 2014. Lessons learned from the fate of AstraZeneca’s drug pipeline: a five-dimensional framework. Nat. Rev. Drug Discov. 13, 419–31.
Costa, P., Sousa Lobo, J.M., 2001. Modeling and comparison of dissolution profiles. Eur. J. Pharm. Sci. 13, 123–133.
Cotte, Y., Toy, F., Jourdain, P., Pavillon, N., Boss, D., Magistretti, P., Marquet, P., Depeursinge, C., 2013. Marker-free phase nanoscopy. Nat. Photonics 7, 113–117.
Cox, E.P., 1927. A Method of Assigning Numerical and Percentage Values to the Degree of Roundness of Sand Grains. J. Paleontol. 1, 179–183.
Curatolo, W., 1998. Physical chemical properties of oral drug candidates in the discovery and exploratory development settings. Pharm. Sci. Technolo. Today 1, 387–393.
Danckwerts, P. V., 1951. Significance of Liquid-Film Coefficients in Gas Absorption. Ind. Eng. Chem. 43, 1460–1467.
Danielsson, L., Zhang, Y., 1996. Methods for determiningn-octanol-water partition constants. TrAC Trends Anal. Chem. 15, 188–196.
de Villiers, M.M., 1996. Influence of agglomeration of cohesive particles on the dissolution behaviour of furosemide powder. Int. J. Pharm. 136, 175–179.
Dejmek, M., Ward, C.A., 1998. A statistical rate theory study of interface concentration during crystal growth or dissolution. J. Chem. Phys. 108, 8698.
Di, L., Fish, P. V, Mano, T., 2012. Bridging solubility between drug discovery and development. Drug Discov. Today 17, 486–95.
Di, L., Kerns, E., Carter, G., 2009. Drug-Like Property Concepts in Pharmaceutical Design. Curr. Pharm. Des. 15, 2184–2194.
Di, L., Kerns, E.H., 2006. Biological assay challenges from compound solubility: strategies for bioassay optimization. Drug Discov. Today 11, 446–51.
DiMasi, J.A., 2002. The Value of Improving the Productivity of the Drug Development Process. Pharmacoeconomics 20, 1–10.
DiMasi, J.A., Hansen, R.W., Grabowski, H.G., 2003. The price of innovation: new estimates of drug development costs. J. Health Econ. 22, 151–85.
Dittert, L.W., Higuchi, T., Reese, D.R., 1964. Phase solubility technique in studying the formation of complex salts of triamterene. J. Pharm. Sci. 53, 1325–1328.
Dressman, J.B., Amidon, G.L., Reppas, C., Shah, V.P., 1998. Dissolution testing as a prognostic tool for oral drug absorption: Immediate release dosage forms. Pharm. Res.
Einstein, A., 1905. Über die von der molekularkinetischen Theorie der Wärme geforderte Bewegung von in ruhenden Flüssigkeiten suspendierten Teilchen. Ann. Phys. 322, 549–560.
Ertl, P., 2003. Cheminformatics analysis of organic substituents: identification of the most common substituents, calculation of substituent properties, and automatic identification of drug-like bioisosteric groups. J. Chem. Inf. Comput. Sci. 43, 374–80.
Faller, B., Ertl, P., 2007. Computational approaches to determine drug solubility. Adv. Drug Deliv. Rev. 59, 533–45.

Fan, X., White, I.M., 2011. Optofluidic microsystems for chemical and biological analysis. Nat. Photonics 5, 591–597.
FDA, 1997. Guidance for Industry: Dissolution Testing of Immediate Release Solid Oral Dosage Forms. Availible at: http://www.fda.gov/downloads/drugs/guidancecomplianceregulatoryinformation/guidances/ucm070237.pdf [Accessed May 13,2016].
Fick, A., 1855. Ueber Diffusion. Ann. der Phys. und Chemie 170, 59–86.
Frank, J., Radermacher, M., Penczek, P., Zhu, J., Li, Y., Ladjadj, M., Leith, A., 1996. SPIDER and WEB: processing and visualization of images in 3D electron microscopy and related fields. J. Struct. Biol. 116, 190–9.
Gamble, J.F., Tobyn, M., Hamey, R., 2015. Application of Image-Based Particle Size and Shape Characterization Systems in the Development of Small Molecule Pharmaceuticals. J. Pharm. Sci. 104, 1563–74.
Gardner, C.R., Walsh, C.T., Almarsson, O., 2004. Drugs as materials: valuing physical form in drug discovery. Nat. Rev. Drug Discov. 3, 926–34.
Gbureck, U., Hölzel, T., Klammert, U., Würzler, K., Müller, F.A., Barralet, J.E., 2007. Resorbable Dicalcium Phosphate Bone Substitutes Prepared by 3D Powder Printing. Adv. Funct. Mater. 17, 3940–3945.
Gerweck, L.E., Kozin, S. V, Stocks, S.J., 1999. The pH partition theory predicts the accumulation and toxicity of doxorubicin in normal and low-pH-adapted cells. Br. J. Cancer 79, 838–42.
Gleeson, M.P., 2008. Generation of a set of simple, interpretable ADMET rules of thumb. J. Med. Chem. 51, 817–34.
Glomme, A., März, J., Dressman, J.B., 2005. Comparison of a miniaturized shake-flask solubility method with automated potentiometric acid/base titrations and calculated solubilities. J. Pharm. Sci. 94, 1–16.
Greenbaum, A., Luo, W., Su, T.-W., Göröcs, Z., Xue, L., Isikman, S.O., Coskun, A.F., Mudanyali, O., Ozcan, A., 2012. Imaging without lenses: achievements and remaining challenges of wide-field on-chip microscopy. Nat. Methods 9, 889–95.
Hamlin, W.E., Northam, J.I., Wagner, J.G., 1965. Relationship betweenin vitro dissolution rates and solubilities of numerous compounds representative of various chemical species. J. Pharm. Sci. 54, 1651–1653.
Hansch, C., Leo, A., Hoekman, D.H., 1995. Exploring QSAR.: Hydrophobic, electronic, and steric constants. American Chemical Society, Washington, DC.
Hansch, C., Quinlan, J.E., Lawrence, G.L., 1968. Linear free-energy relationship between partition coefficients and the aqueous solubility of organic liquids. J. Org. Chem. 33, 347–350.
Heikkilä, T., Karjalainen, M., Ojala, K., Partola, K., Lammert, F., Augustijns, P., Urtti, A., Yliperttula, M., Peltonen, L., Hirvonen, J., 2011. Equilibrium drug solubility measurements in 96-well plates reveal similar drug solubilities in phosphate buffer pH 6.8 and human intestinal fluid. Int. J. Pharm. 405, 132–6.
Hell, S.W., 2007. Far-field optical nanoscopy. Science 316, 1153–8.
Higuchi, W.I., 1967. Diffusional models useful in biopharmaceutics. Drug release rate processes. J. Pharm. Sci. 56, 315–324.
Higuchi, W.I., Hiestand, E.N., 1963. Dissolution Rates of Finely Divided Drug Powders I. J. Pharm. Sci. 52, 67–71.
Higuchi, W.I., Parker, A.P., Hamlin, W.E., 1965. Dissolution kinetics of a weak acid, 1,1-hexamethylene p-tolylsulfonylsemicarbazide, and its sodium salt. J. Pharm. Sci. 54, 8–11.
Hintz, R., Johnson, K., 1989. The effect of particle size distribution on dissolution rate and oral absorption. Int. J. Pharm. 51, 9–17.
Hixson, A.W., Crowell, J.H., 1931. Dependence of Reaction Velocity upon surface and Agitation. Ind. Eng. Chem. 23, 923–931.
Hopfinger, A.J., Esposito, E.X., Llinàs, A., Glen, R.C., Goodman, J.M., 2009. Findings of the Challenge To Predict Aqueous Solubility. J. Chem. Inf. Model. 49, 1–5.
Huang, L.-F., Tong, W.-Q., 2004. Impact of solid state properties on developability assessment of drug candidates. Adv. Drug Deliv. Rev. 56, 321–34.

Hughes, J.D., Blagg, J., Price, D.A., Bailey, S., Decrescenzo, G.A., Devraj, R. V, Ellsworth, E., Fobian, Y.M., Gibbs, M.E., Gilles, R.W., Greene, N., Huang, E., Krieger-Burke, T., Loesel, J., Wager, T., Whiteley, L., Zhang, Y., 2008. Physiochemical drug properties associated with in vivo toxicological outcomes. Bioorg. Med. Chem. Lett. 18, 4872–5.

Hulse, W.L., Gray, J., Forbes, R.T., 2012. A discriminatory intrinsic dissolution study using UV area imaging analysis to gain additional insights into the dissolution behaviour of active pharmaceutical ingredients. Int. J. Pharm. 434, 133–9.

Israelachvili, J.N., 1992. Intermolecular and Surface Forces, 2nd ed. Academic Press, London.

Jain, N., Yalkowsky, S.H., 2001. Estimation of the aqueous solubility I: application to organic nonelectrolytes. J. Pharm. Sci. 90, 234–52.

Jorgensen, W.L., Duffy, E.M., 2002. Prediction of drug solubility from structure. Adv. Drug Deliv. Rev. 54, 355–366.

Katritzky, A.R., Wang, Y., Sild, S., Tamm, T., Karelson, M., 1998. QSPR Studies on Vapor Pressure, Aqueous Solubility, and the Prediction of Water–Air Partition Coefficients. J. Chem. Inf. Comput. Sci. 38, 720–725.

Kerns, E.H., 2001. High throughput physicochemical profiling for drug discovery. J. Pharm. Sci. 90, 1838–58.

Kerns, E.H., Di, L., 2008. Drug-like Properties: Concepts, Structure Design and Methods. Academic Press, Burlington.

Keserü, G.M., Makara, G.M., 2009. The influence of lead discovery strategies on the properties of drug candidates. Nat. Rev. Drug Discov. 8, 203–212.

Klein, S., Shah, V.P., 2008. A standardized mini paddle apparatus as an alternative to the standard paddle. AAPS PharmSciTech 9, 1179–84.

Kola, I., Landis, J., 2004. Can the pharmaceutical industry reduce attrition rates? Nat. Rev. Drug Discov. 3, 711–5.

Korfmacher, W.A., 2005. Principles and applications of LC-MS in new drug discovery. Drug Discov. Today 10, 1357–67.

Kröner, S., Doménech Carbó, M.T., 2013. Determination of minimum pixel resolution for shape analysis: Proposal of a new data validation method for computerized images. Powder Technol. 245, 297–313.

Leeson, P.D., Springthorpe, B., 2007. The influence of drug-like concepts on decision-making in medicinal chemistry. Nat. Rev. Drug Discov. 6, 881–90.

Lehto, P., Aaltonen, J., Niemelä, P., Rantanen, J., Hirvonen, J., Tanninen, V.P., Peltonen, L., 2008. Simultaneous measurement of liquid-phase and solid-phase transformation kinetics in rotating disc and channel flow cell dissolution devices. Int. J. Pharm. 363, 66–72.

Levich, V., 1962. Physicochemical Hydrodynamics. Prentice Hall, New Jersey.

Lewis, D.F. V, Dickins, M., 2003. Baseline lipophilicity relationships in human cytochromes P450 associated with drug metabolism. Drug Metab. Rev. 35, 1–18.

Linnankoski, J., Mäkelä, J.M., Ranta, V.-P., Urtti, A., Yliperttula, M., 2006. Computational prediction of oral drug absorption based on absorption rate constants in humans. J. Med. Chem. 49, 3674–81.

Lipinski, C.A., 2001. Avoiding investment in doomed drugs, is poor solubility an industry wide problem? Curr. Drug Discov. 1, 17–19.

Lipinski, C.A., Lombardo, F., Dominy, B.W., Feeney, P.J., 1997. Experimental and computational approaches to estimate solubility and permeability in drug discovery and development settings. Adv. Drug Deliv. Rev. 23, 3–25.

Löbmann, K., Flouda, K., Qiu, D., Tsolakou, T., Wang, W., Rades, T., 2014. The influence of pressure on the intrinsic dissolution rate of amorphous indomethacin. Pharmaceutics 6, 481–93.

Lombardo, F., Shalaeva, M.Y., Tupper, K.A., Gao, F., Abraham, M.H., 2000. ElogP oct : A Tool for Lipophilicity Determination in Drug Discovery †. J. Med. Chem. 43, 2922–2928.

Mannhold, R., Poda, G.I., Ostermann, C., Tetko, I. V, 2009. Calculation of molecular lipophilicity: State-of-the-art and comparison of log P methods on more than 96,000 compounds. J. Pharm. Sci. 98, 861–93.

Marabi, A., Mayor, G., Burbidge, A., Wallach, R., Saguy, I., 2008. Assessing dissolution kinetics

of powders by a single particle approach. Chem. Eng. J. 139, 118–127.
Marx, V., 2012. Digging deep and wide into single cells. Nat. Methods 9, 1151–1155.
Massera, J., Hupa, L., 2014. Influence of SrO substitution for CaO on the properties of bioactive glass S53P4. J. Mater. Sci. Mater. Med. 25, 657–68.
Merkle, H.P., Jen, A., 2002. A crystal clear solution for insulin delivery. Nat. Biotechnol. 20, 789–90.
Morgan, P., Van Der Graaf, P.H., Arrowsmith, J., Feltner, D.E., Drummond, K.S., Wegner, C.D., Street, S.D.A., 2012. Can the flow of medicines be improved? Fundamental pharmacokinetic and pharmacological principles toward improving Phase II survival. Drug Discov. Today 17, 419–24.
Morphy, R., 2006. The influence of target family and functional activity on the physicochemical properties of pre-clinical compounds. J. Med. Chem. 49, 2969–78.
Mosharraf, M., Nyström, C., 1995. The effect of particle size and shape on the surface specific dissolution rate of microsized practically insoluble drugs. Int. J. Pharm. 122, 35–47.
Mullard, A., 2016. 2015 FDA drug approvals. Nat. Rev. Drug Discov. 15, 73–6.
Munos, B., 2009. Lessons from 60 years of pharmaceutical innovation. Nat. Rev. Drug Discov. 8, 959–68.
Murphy, L.R., Matubayasi, N., Payne, V.A., Levy, R.M., 1998. Protein hydration and unfolding--insights from experimental partial specific volumes and unfolded protein models. Fold. Des. 3, 105–18.
Nernst, W., 1904. Theorie der Reaktionsgeschwindigkeit in heterogenen Systemen. Zeitschrift für Phys. Chemie, Stoechiom. und Verwandtschaftslehre 47, 52 – 55.
Niebergall, P.J., Milosovich, G., Goyan, J.E., 1963. Dissolution Rate Studies II. J. Pharm. Sci. 52, 236–241.
Nilsson, J., Evander, M., Hammarström, B., Laurell, T., 2009. Review of cell and particle trapping in microfluidic systems. Anal. Chim. Acta 649, 141–57.
Noyes, A.A., Whitney, W.R., 1897. The rate of solution of solid substances in their own solutions. J. Am. Chem. Soc. 19, 930–934.
O'Neil, M.J., 2001. The Merck Index: An Encyclopedia Of Chemicals, Drugs, And Biologicals, 13th ed. Merck Research Laboratories, Whitehouse Station.
OECD, 2016a. OECD Guidelines for the Testing of Chemicals, Section 1, Test No. 105: Water Solubility. Available at: http://www.oecd-ilibrary.org/environment/test-no-105-water-solubility_9789264069589-en [Accessed March 5, 2016].
OECD, 2016b. OECD Guidelines for the Testing of Chemicals, Section 1, Test No. 107: Partition Coefficient (n-octanol/water): Shake Flask Method. Available at: http://www.oecd-ilibrary.org/environment/test-no-107-partition-coefficient-n-octanol-water-shake-flask-method_9789264069626-en [Accessed March 5, 2016].
Østergaard, J., Lenke, J., Sun, Y., Ye, F., 2014. UV Imaging for In Vitro Dissolution and Release Studies: Intial Experiences. Dissolution Technol. 21, 27–38.
Østergaard, J., Ye, F., Rantanen, J., Yaghmur, A., Larsen, S.W., Larsen, C., Jensen, H., 2011. Monitoring lidocaine single-crystal dissolution by ultraviolet imaging. J. Pharm. Sci. 100, 3405–10.
Ostwald, W., 1897. Studien Über Die Bildung und Umwandlung Fester Körper. Zeitschrift für Phys. Chemie. 22, 289-330.
Paakkunainen, M., Matero, S., Ketolainen, J., Lahtela-Kakkonen, M., Poso, A., Reinikainen, S.-P., 2009. Uncertainty in dissolution test of drug release. Chemom. Intell. Lab. Syst. 97, 82–90.
Parrott, E.L., Wurster, D.E., Higuchi, T., 1955. Investigation of drug release from solids. I. Some factors influencing the dissolution rate. J. Am. Pharm. Assoc. 44, 269–273.
Paul, S.M., Mytelka, D.S., Dunwiddie, C.T., Persinger, C.C., Munos, B.H., Lindborg, S.R., Schacht, A.L., 2010. How to improve R&D productivity: the pharmaceutical industry's grand challenge. Nat. Rev. Drug Discov. 9, 203–14.
Ph.Eur., 2015. 4.01.03 Buffer solutions. Eur. Pharmacopoeia Online 8.8. Available at: http://online6.edqm.eu/ep808/ [Accessed January 3, 2016].
Ploemen, J.-P.H.T.M., Kelder, J., Hafmans, T., van de Sandt, H., van Burgsteden, J.A., Salemink, P.J.M., van Esch, E., 2004. Use of physicochemical calculation of pKa and

CLogP to predict phospholipidosis-inducing potential. Exp. Toxicol. Pathol. 55, 347–355.
Podczeck, F., 1997. A shape factor to assess the shape of particles using image analysis. Powder Technol. 93, 47–53.
Podczeck, F., 1995. The evaluation of a three-dimensional shape factor for the quantitative assessment of the sphericity and surface roughness of pellets. Int. J. Pharm. 124, 253–259.
Poole, S.K., Durham, D., Kibbey, C., 2000. Rapid method for estimating the octanol–water partition coefficient (log Pow) by microemulsion electrokinetic chromatography. J. Chromatogr. B Biomed. Sci. Appl. 745, 117–126.
Popa-Burke, I.G., Issakova, O., Arroway, J.D., Bernasconi, P., Chen, M., Coudurier, L., Galasinski, S., Jadhav, A.P., Janzen, W.P., Lagasca, D., Liu, D., Lewis, R.S., Mohney, R.P., Sepetov, N., Sparkman, D.A., Hodge, C.N., 2004. Streamlined system for purifying and quantifying a diverse library of compounds and the effect of compound concentration measurements on the accurate interpretation of biological assay results. Anal. Chem. 76, 7278–87.
Prasad, K.V.R., Ristic, R.I., Sheen, D.B., Sherwood, J.N., 2002. Dissolution kinetics of paracetamol single crystals. Int. J. Pharm. 238, 29–41.
Pudipeddi, M., Serajuddin, A.T.M., 2005. Trends in solubility of polymorphs. J. Pharm. Sci. 94, 929–39.
Raghavan, S.L., Ristic, R.I., Sheen, D.B., Sherwood, J.N., 2002. Dissolution kinetics of single crystals of alpha-lactose monohydrate. J. Pharm. Sci. 91, 2166–74.
Ran, Y., Jain, N., Yalkowsky, S.H., 2001. Prediction of Aqueous Solubility of Organic Compounds by the General Solubility Equation (GSE). J. Chem. Inf. Comput. Sci. 41, 1208–1217.
Sacher, F., Lange, F.T., Brauch, H.-J., Blankenhorn, I., 2001. Pharmaceuticals in groundwaters. J. Chromatogr. A 938, 199–210.
Saunders, K.C., 2004. Automation and robotics in ADME screening. Drug Discov. Today. Technol. 1, 373–80.
Scherrer, R.A., Howard, S.M., 1977. Use of distribution coefficients in quantitative structure-activity relations. J. Med. Chem. 20, 53–58.
Schmidt, H., Hawkins, A.R., 2011. The photonic integration of non-solid media using optofluidics. Nat. Photonics 5, 598–604.
Serajuddin, A.T.M., Jarowski, C.I., 1985. Effect of Diffusion Layer pH and Solubility on the Dissolution Rate of Pharmaceutical Acids and Their Sodium Salts II: Salicylic Acid, Theophylline, and Benzoic Acid. J. Pharm. Sci. 74, 148–154.
Shah, A.C., Nelson, K.G., 1975. Evaluation of a convective diffusion drug dissolution rate model. J. Pharm. Sci. 64, 1518–1520.
Slater, B., McCormack, A., Avdeef, A., Comer, J.E.A., 1994. PH-Metric logP.4. Comparison of Partition Coefficients Determined by HPLC and Potentiometric Methods to Literature Values. J. Pharm. Sci. 83, 1280–1283.
Smietana, K., Ekstrom, L., Jeffery, B., Møller, M., 2015. Improving R&D productivity. Nat. Rev. Drug Discov. 14, 455–6.
Sousa, J.J., Sousa, A., Podczeck, F., Newton, J.M., 2002. Factors influencing the physical characteristics of pellets obtained by extrusion-spheronization. Int. J. Pharm. 232, 91–106.
Stuart, M., Box, K., 2005. Chasing Equilibrium: Measuring the Intrinsic Solubility of Weak Acids and Bases. Anal. Chem. 77, 983–990.
Sugano, K., Kato, T., Suzuki, K., Keiko, K., Sujaku, T., Mano, T., 2006. High throughput solubility measurement with automated polarized light microscopy analysis. J. Pharm. Sci. 95, 2115–22.
Sugano, K., Okazaki, A., Sugimoto, S., Tavornvipas, S., Omura, A., Mano, T., 2007. Solubility and Dissolution Profile Assessment in Drug Discovery. Drug Metab. Pharmacokinet. 22, 225–254.
Takács-Novák, K., Box, K.J., Avdeef, A., 1997. Potentiometric pKa determination of water-insoluble compounds: validation study in methanol/water mixtures. Int. J. Pharm. 151, 235–248.

Ternes, T.A., 2001. Analytical methods for the determination of pharmaceuticals in aqueous environmental samples. TrAC Trends Anal. Chem. 20, 419–434.
Tetko, I. V., Poda, G.I., Ostermann, C., Mannhold, R., 2009. Accurate In Silico log P Predictions: One Can't Embrace the Unembraceable. QSAR Comb. Sci. 28, 845–849.
Tiller, P.R., Romanyshyn, L.A., Neue, U.D., 2003. Fast LC/MS in the analysis of small molecules. Anal. Bioanal. Chem. 377, 788–802.
Tomizawa, K., Sugano, K., Yamada, H., Horii, I., 2006. Physicochemical and cell-based approach for early screening of phospholipidosis-inducing potential. J. Toxicol. Sci. 31, 315–24.
Tong, C., Lozano, R., Mao, Y., Mirza, T., Löbenberg, R., Nickerson, B., Gray, V., Wang, Q., 2009. The value of in Vitro dissolution in drug development: A position paper from the AAPS in Vitro release and dissolution focus group. Pharm. Technol. 33, 52–64.
Tsinman, K., Avdeef, A., Tsinman, O., Voloboy, D., 2009. Powder dissolution method for estimating rotating disk intrinsic dissolution rates of low solubility drugs. Pharm. Res. 26, 2093–100.
Tsuji, A., Nakashima, E., Hamano, S., Yamana, T., 1978. Physicochemical properties of amphoteric beta-lactam antibiotics I: Stability, solubility, and dissolution behavior of amino penicillins as a function of pH. J. Pharm. Sci. 67, 1059–1066.
US National Library of Medicine, 2014. ChemIDplus Advanced Online Database. Available at: http://chem.sis.nlm.nih.gov/chemidplus/ [Accessed January 4, 2015].
USP, 2015. United States Pharmacopoeia XXIV Pharmacopoeia XXIV. US Pharmacopeia Convention, Inc., Rockville.
Valkó, K., 1997. Chromatographic hydrophobicity index by fast-gradient RP-HPLC: A high-throughput alternative to log P/log D. Anal. Chem. 69, 2022–2029.
Valko, K., Nunhuck, S., Bevan, C., Abraham, M.H., Reynolds, D.P., 2003. Fast gradient HPLC method to determine compounds binding to human serum albumin. Relationships with octanol/water and immobilized artificial membrane lipophilicity. J. Pharm. Sci. 92, 2236–48.
Veber, D.F., Johnson, S.R., Cheng, H.-Y., Smith, B.R., Ward, K.W., Kopple, K.D., 2002. Molecular Properties That Influence the Oral Bioavailability of Drug Candidates. J. Med. Chem. 45, 2615–2623.
Wang, J., Flanagan, D.R., 1999. General solution for diffusion-controlled dissolution of spherical particles. 1. Theory. J. Pharm. Sci. 88, 731–8.
Waring, M.J., 2010. Lipophilicity in drug discovery. Expert Opin. Drug Discov. 5, 235–48.
Waring, M.J., Arrowsmith, J., Leach, A.R., Leeson, P.D., Mandrell, S., Owen, R.M., Pairaudeau, G., Pennie, W.D., Pickett, S.D., Wang, J., Wallace, O., Weir, A., 2015. An analysis of the attrition of drug candidates from four major pharmaceutical companies. Nat. Rev. Drug Discov. 14, 475–486.
Waring, M.J., Johnstone, C., 2007. A quantitative assessment of hERG liability as a function of lipophilicity. Bioorg. Med. Chem. Lett. 17, 1759–64.
Weiss, T.F., 1996. Cellular Biophysics,Vol. 1. MIT Press, Cambridge.
Wenlock, M.C., Austin, R.P., Barton, P., Davis, A.M., Leeson, P.D., 2003. A comparison of physiochemical property profiles of development and marketed oral drugs. J. Med. Chem. 46, 1250–6.
Winiwarter, S., Bonham, N.M., Ax, F., Hallberg, A., Lennernäs, H., Karlén, A., 1998. Correlation of human jejunal permeability (in vivo) of drugs with experimentally and theoretically derived parameters. A multivariate data analysis approach. J. Med. Chem. 41, 4939–49.
Wu, J., Berg, F., Rantanen, J., Rades, T., Yang, M., 2014. Current Advances and Future Trends in Characterizing Poorly Water-soluble Drugs Using Spectroscopic, Imaging and Data Analytical Techniques. Curr. Pharm. Des. 20, 436–453.
Wurster, D.E., Taylor, P.W., 1965. Dissolution rates. J. Pharm. Sci. 54, 169–175.
Yalkowsky, S.H., Valvani, S.C., 1980. Solubility and partitioning I: Solubility of nonelectrolytes in water. J. Pharm. Sci. 69, 912–922.
Yu, L.X., 1999. An integrated model for determining causes of poor oral drug absorption. Pharm. Res. 16, 1883–1887.

Yu, L.X., Carlin, A.S., Amidon, G.L., Hussain, A.S., 2004. Feasibility studies of utilizing disk intrinsic dissolution rate to classify drugs. Int. J. Pharm. 270, 221–227.

Zakeri-Milani, P., Barzegar-Jalali, M., Azimi, M., Valizadeh, H., 2009. Biopharmaceutical classification of drugs using intrinsic dissolution rate (IDR) and rat intestinal permeability. Eur. J. Pharm. Biopharm. 73, 102–6.